Fluorescence Polarization Transients from Rhodamine Isomers on the Myosin Regulatory Light Chain in Skeletal Muscle Fibers

Seth C. Hopkins,* Cibele Sabido-David,# John E.T. Corrie,§ Malcolm Irving,# and Yale E. Goldman*
*Pennsylvania Muscle Institute, University of Pennsylvania, Philadelphia, Pennsylvania 19104-6083, USA; #Randall Institute, King's College London, London WC2B 5RL, England; and §National Institute for Medical Research, London NW7 1AA, England

ABSTRACT Fluorescence polarization was used to examine orientation changes of two rhodamine probes bound to myosin heads in skeletal muscle fibers. Chicken gizzard myosin regulatory light chain (RLC) was labeled at Cys^{108} with either the 5- or the 6-isomer of iodoacetamidotetramethylrhodamine (IATR). Labeled RLC (termed $Cys^{108\text{-}5}$ or $Cys^{108\text{-}6}$) was exchanged for the endogenous RLC in single, skinned fibers from rabbit psoas muscle. Three independent fluorescence polarization ratios were used to determine the static angular distribution of the probe dipoles with respect to the fiber axis and the extent of probe motions on the nanosecond time scale of the fluorescence lifetime. We used step changes in fiber length to partially synchronize the transitions between biochemical, structural, and mechanical states of the myosin cross-bridges. Releases during active contraction tilted the $Cys^{108\text{-}6}$ dipoles away from the fiber axis. This response saturated for releases beyond 3 nm/half-sarcomere (h.s.). Stretches in active contraction caused the dipoles to tilt toward the fiber axis, with no evidence of saturation for stretches up to 7 nm/h.s. These nonlinearities of the response to length changes are consistent with a partition of ~90% of the probes that did not tilt when length changes were applied and 10% of the probes that tilted. The responding fraction tilted ~30° for a 7.5 nm/h.s. release and traversed the plane perpendicular to the fiber axis for larger releases. Stretches in rigor tilted $Cys^{108\text{-}6}$ dipoles away from the fiber axis, which was the opposite of the response in active contraction. The transition from the rigor-type to the active-type response to stretch preceded the main force development when fibers were activated from rigor by photolysis of caged ATP in the presence of Ca^{2+}. Polarization ratios for $Cys^{108\text{-}6}$ in low ionic strength (20 mM) relaxing solution were compatible with a combination of the relaxed (200 mM ionic strength) and rigor intensities, but the response to length changes was of the active type. The nanosecond motions of the $Cys^{108\text{-}6}$ dipole were restricted to a cone of ~20° half-angle, and those of $Cys^{108\text{-}5}$ dipole to a cone of ~25° half-angle. These values changed little between relaxation, active contraction, and rigor. $Cys^{108\text{-}5}$ showed very small-amplitude tilting toward the fiber axis for both stretches and releases in active contraction, but much larger amplitude tilting in rigor. The marked differences in these responses to length steps between the two probe isomers and between active contraction and rigor suggest that the RLC undergoes a large angle change (~60°) between these two states. This motion is likely to be a combination of tilting of the RLC relative to the fiber axis and twisting of the RLC about its own axis.

INTRODUCTION

Several recent studies have provided support for the hypothesis that the light chain region of the myosin head tilts during the power stroke of the cross-bridge cycle in muscle contraction (Whittaker et al., 1995; Irving et al., 1995; Gollub et al., 1996). Myosin subfragment 1 (S1) has been shown by x-ray crystallography to be composed of a catalytic domain containing the nucleotide and actin binding sites, and a light chain binding domain (Rayment et al., 1993b). Models of S1 bound to filamentous actin in the absence of ATP (Rayment et al., 1993a) suggest that the catalytic domain binds rigidly and stereospecifically to actin, but that the N-terminal α-helix with its associated essential and regulatory light chains might form a mechanical lever arm (Rayment et al., 1993a; Lowey et al., 1993; VanBuren et al., 1994; Uyeda et al., 1996) that amplifies small motions within the catalytic domain into a 5–10-nm translation at the junction between S1 and the myosin rod (Huxley and Simmons, 1971; Finer et al., 1994; Molloy et al., 1995). Although many studies have identified internal flexion within myosin and rotational motions of the head, it has been difficult to correlate these motions with the force-generating transition (Morales et al., 1982; Cooke et al., 1984; Tanner et al., 1992). The heterogeneity of biochemical states, the orientational disorder of the myosin heads, and the unknown angle and disorder of extrinsic probes relative to the heads have contributed to this difficulty (Ostap et al., 1995; Berger et al., 1996).

Recently, several studies have correlated motions of myosin with force generation. Irving et al. (1992) and Lombardi et al. (1995) monitored x-ray diffraction patterns with high time resolution in single, live muscle fibers during mechanical transients initiated by quick length steps. They found intensity changes of the myosin-based 14.5-nm meridional reflection concomitant with quick length changes and the subsequent force recovery, and they interpreted these deflections on the basis of tilting motions of the myosin heads. Irving et al. (1995) monitored orientation changes of rhodamine probes bound to the regulatory light chain (RLC) region of the myosin head during mechanical

Received for publication 10 September 1997 and in final form 22 January 1998.

Address reprint requests to Dr. Yale E. Goldman, Department of Physiology, University of Pennsylvania School of Medicine, D-700 Richards Building, 3700 Hamilton Walk, Philadelphia, PA 19104-6083. Tel.: 215-898-4017; Fax: 215-898-2653; E-mail: goldmany@mail.med.upenn.edu.

0006-3495/98/06/3093/18 $2.00

transients, thereby localizing the motions to that part of S1. The polarization signals changed during the length steps applied in active contraction and in rigor, signaling the elastic properties of the myosin heads. In contracting fibers the polarization signals changed further during the quick tension recovery after the length step. The rates of this further change in polarization signals and of the quick tension recovery were comparable, suggesting that tilting accompanies the power stroke. In contrast, probes bound to SH1 (Cys^{707} of the heavy chain) in the catalytic domain of S1 did not tilt in response to length changes (Berger et al., 1996). Burghardt et al. (1997) observed very small deflections of fluorescence polarization ratios from probes predominantly bound to Cys^{707} when length changes were applied to fibers. These deflections were an order of magnitude smaller than those seen with RLC probes (Irving et al., 1995). Together these results suggest an internal flexing of the myosin head.

Although the data of Irving et al. (1995) suggested a large angular change between active contraction and rigor, a change of only 3°–5° averaged over the whole population of probes was observed after a 3-nm release during contraction. Several factors could reduce the amplitude of the angular change associated with active length steps. First, the fluorescence polarization technique is not sensitive to azimuthal motions. Moreover, if the working stroke motion is in a plane and probe dipoles are oriented away from this plane, then the tilting of the probe transition moment would be reduced. In the limiting case, with the probe dipoles perpendicular to the plane of the motion, no tilting would be detected. If some myosin heads are in mechanical or biochemical states that do not respond to the length changes (e.g., because they are detached from actin), the tilting motion of the remaining ("active") heads would be correspondingly greater than the average. Heterogeneity or rapid motions of the probes relative to the myosin heads might also reduce the observed tilt angle. These factors must be determined experimentally.

The problem of the angle between the probe dipole and the plane of the working stroke can be addressed by using different isomers of the probe that might interact with the heads at differing orientations in the neighborhood of their linking residue. Ling et al. (1996) and Allen et al. (1996) used a commercial sample of iodoacetamidotetramethylrhodamine (IATR), of unknown isomer composition and purity, to label RLC from rabbit skeletal and chicken gizzard muscle. In the experiments of Irving et al. (1995), chicken gizzard RLC was labeled with pure 6-isomer of IATR (Corrie and Craik, 1994). The labeled RLC was further purified by fast protein liquid chromatography (FPLC) and exchanged into glycerol-extracted psoas fibers from rabbit muscle. When similar experiments were performed with gizzard RLC, labeled with the pure 5-IATR, the static fluorescence polarization values from muscle fibers were very different from those obtained with the pure 6-isomer (Sabido-David et al., 1998a, accompanying paper). In rigor the two dipoles had orientations more than 20° apart. The 6-isomer was more perpendicular to the muscle fiber axis than the 5-isomer. The 6-isomer showed marked changes between rigor and active contraction, whereas the 5-isomer showed smaller changes between these states.

We therefore set out to characterize the polarization transients from these two isomers after application of quick length changes to the muscle fibers. We also developed a method of estimating the extent of probe wobble on the nanosecond time scale of the fluorescence lifetime. These motions can be separated from slower motions of the proteins and static disorder in the angular distribution (Irving, 1996). We studied fluorescence polarization transients produced by length changes in active contraction and in rigor and characterized their dependence on the amplitude of the length changes. To relate these length step transients to the biochemical steps of the cross-bridge cycle, we studied fibers relaxed at low temperature and low ionic strength and measured fluorescence polarization changes after photolysis of caged ATP in fibers containing RLC labeled with the pure 6-isomer of IATR. Some results of these experiments have been presented in abstract form (Hopkins et al., 1995, 1996a).

MATERIALS AND METHODS

Chemicals and solutions

Experimental solution compositions are shown in Table 1. All experiments were done at 13° ± 2°C, except where noted (Fig. 7 and associated text).

TABLE 1 Solutions used

Solution	EGTA	CaEGTA	HDTA	Na_2ATP	Na_2CP	$MgCl_2$
Relax, 5 mM MgATP	25			5.4	19.1	7.7
Relax, 0.1 mM MgATP	36.5			0.1	20	2.8
Rigor	56.3					2.5
Ca^{2+} rigor		20	34.3			1.2
Preactivating	0.1		24.9	5.6	19.5	6.9
Activating		25		5.6	22.3	6.9

All concentrations are in mM. All solutions, unless otherwise noted, contained 100 mM TES, 10 mM reduced glutathione, 1 mM calculated free Mg^{2+}, 200 mM ionic strength, and pH 7.1 at 10°C. Relaxing, preactivating, and activating solutions contained 1 mg/ml creatine phosphokinase (~100–200 units/mg activity). For photolysis solutions, concentrated rigor stock solutions, caged ATP, and H_2O were combined to yield the above concentrations and 10 mM caged ATP. Relaxing solution at 0.02 M ionic strength, 3°C, contained 2 mM EGTA, 1.06 mM CP, 2.1 mM Mg acetate, 0.68 mM K acetate, and 7 mM imidazole. Ca-EGTA contains the same concentrations of total Ca and EGTA; TES, *N*-Tris(hydroxymethyl)methyl-2-aminoethanesulfonic acid; CP, creatine phosphate; caged ATP, P^3-1-(2-nitrophenyl)ethyladenosine-5′-triphosphate; HDTA, 1,6-diaminohexane-*N,N,N′,N′*-tetraacetic acid.

All reagents, unless otherwise noted, were analytical grade. Nucleotides were obtained from Sigma Chemical Company (St. Louis, MO). Caged ATP was synthesized as described by Walker et al. (1989). The 5- and 6-isomers of IATR were synthesized as described previously (Corrie and Craik, 1994).

Fiber preparation and incorporation of labeled RLC

Bundles of rabbit psoas muscle fibers were dissected, skinned with glycerol, and stored as previously described (Goldman et al., 1984a). Chicken gizzard myosin RLC (a kind gift from Dr. J. Kendrick-Jones) was labeled with the 5- or 6-isomer of IATR and then purified by Ms. Birgit Brandmeier and Dr. D.R. Trentham by FPLC (Sabido-David et al., 1998a). The labeled RLC used here was homogeneous to >95% by reverse-phase high-pressure liquid chromatography (HPLC). It was exchanged into single glycerol-extracted psoas fibers by using a low-Mg rigor solution followed by incubation of the fibers in troponin and troponin-C solutions, to replace components lost in the RLC exchange step as described by Sabido-David et al. (1998a).

Experimental apparatus

The apparatus for mechanical measurements on single, skinned muscle fibers, application of rapid length changes, and photolysis of caged nucleotides was similar to that described by Goldman et al. (1984a) and Allen et al. (1996). Single muscle fibers were dissected from bundles stored in glycerol. Short segments (2–3 mm) were cut, and aluminum T-clips were attached to their ends. The regions of the fiber inside and within ~50 μm of the T-clips were fixed by glutaraldehyde to limit end compliance (modified from Chase and Kushmerick, 1988). A muscle fiber segment was mounted via the T-clips to hooks on a strain gauge force transducer (Sensonor, Norway; natural frequency 5 kHz) at one end, and a moving coil motor (Cecchi et al., 1976; Lombardi and Piazzesi, 1990) designed to produce rapid length steps at the other end. The two hooks were carefully aligned under a binocular microscope and then moved apart on two parallel dovetail slides to ensure that the fiber axis was perpendicular to the optical axes. The fiber was bathed in experimental solutions contained in interchangeable stainless steel troughs (Fig. 1). Resting sarcomere lengths and fiber dimensions were determined as described by Goldman and Simmons (1984). Timing of applied length changes and triggering of the recordings were controlled by a programmable timing generator based on a Z8 microprocessor (Ciarcia, 1981a, b).

Fluorescence polarization data were acquired as described by Allen et al. (1996), except that a second illumination pathway was added to the setup to obtain additional information about the probe orientational distribution. Fig. 1 shows the optical geometry. A continuous 100-mW, 514.5-nm argon laser (model 5500A; ILT, Salt Lake City, UT) was used to excite rhodamine fluorescence. The polarization of the exciting light was modulated at 84.2 kHz by a photoelastic modulator (PEM-80 model FSA; Hinds International, Portland, OR). A cylindrical lens compressed the

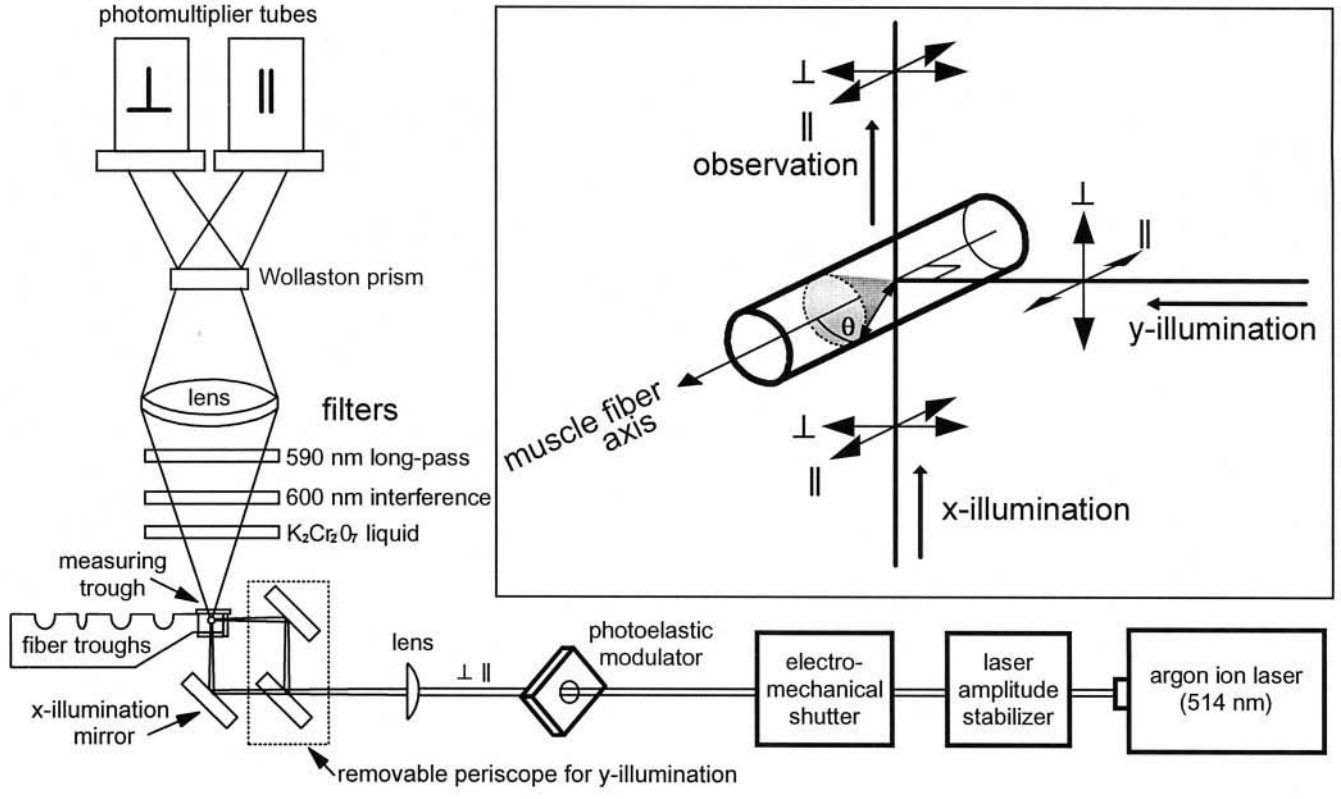

FIGURE 1 Schematic diagram of the optical set-up for measuring fluorescence polarization. The muscle fiber was mounted in the measuring trough with its long axis normal to the plane of the diagram. The periscope was removed for *x* illumination (in line with the detector). Light polarized normal to the plane of the diagram is parallel to the fiber axis. The perspective view (*inset*) shows the propagation of *x* illumination and *y* illumination, the direction of fluorescence observation, and the orientations of the excitation and emission polarizations relative to the fiber axis. With the periscope removed, the same arrangement could be used to photolyze caged ATP in the measuring trough with a pulse of ultraviolet light (not shown) passing through a fused silica window from the direction of *y* illumination (Tanner et al., 1992). Emission filters were a 1-cm path length 100 mM $K_2Cr_2O_7$ solution in a fused silica cuvette to block phosphorescence emission from the glass in the optical path, and a 590-nm glass cut-off filter (Schott Glass Technologies, Duryea, PA) to remove green laser light. In experiments that included photolysis of caged ATP, an interference filter (600 nm, 40 nm FWHM; Melles Griot, Irvine, CA) was placed in the emission path to block scattered UV light. The effective numerical aperture of the collecting lens was 0.3.

beam to ~100 μm across the fiber diameter. A ~2-mm length of the muscle fiber was illuminated at 20–30 mW total power either from below (termed *x* illumination) or from the side (*y* illumination) through the fused silica windows of the measuring trough. A periscope mirror (Fig. 1) was in place for *y* illumination and removed for *x* illumination. An electromechanical shutter in the excitation path, operated by the timing generator, opened only during data recording, reducing photobleaching to less than ~20% in most experiments. The fluorescence, collected by a lens and spectral filters, was separated into parallel and perpendicular components by a Wollaston prism, and detected by two photomultiplier tubes (model R928; Hamamatsu, Bridgewater, NJ). The parallel and perpendicular fluorescence signals were digitized together with tension and motor position at 12-bit resolution and a 2-μs sampling interval by a digital oscilloscope (Pro 40; Nicolet, Madison, WI). In a typical experimental trial, the signals were recorded for 480 ms, giving ~2 Mbytes of data, which were transferred to a 80486-based computer through a IEEE-488 bus and stored on 90-Mbyte Bernoulli cartridges (Iomega, South Roy, UT), using software written in-house. Tension, motor position, and four optical signals ($D_\parallel$, $D_\perp$, $L_\parallel$, and $L_\perp$, described below) were simultaneously sampled every 500 μs, digitized at 12-bit resolution, and stored on disk using a 80386-based computer. During separate activations, sarcomere length deflections during the imposed length steps were measured by white light diffraction (Goldman, 1987) and recorded at both sampling rates.

Processing of fluorescence intensity data

Four fluorescence polarization ratios were defined as

$$
\begin{aligned}
{}^{x}Q_\parallel &= {}^{x}D_\parallel/{}^{x}L_\parallel = ({}^{x}_\parallel I_\parallel - {}^{x}_\perp I_\parallel)/({}^{x}_\parallel I_\parallel + {}^{x}_\perp I_\parallel)\\
{}^{x}Q_\perp &= {}^{x}D_\perp/{}^{x}L_\perp = ({}^{x}_\perp I_\perp - {}^{x}_\parallel I_\perp)/({}^{x}_\perp I_\perp + {}^{x}_\parallel I_\perp)\\
{}^{y}Q_\parallel &= {}^{y}D_\parallel/{}^{y}L_\parallel = ({}^{y}_\parallel I_\parallel - {}^{y}_\perp I_\parallel)/({}^{y}_\parallel I_\parallel + {}^{y}_\perp I_\parallel)\\
{}^{y}Q_\perp &= {}^{y}D_\perp/{}^{y}L_\perp = ({}^{y}_\perp I_\perp - {}^{y}_\parallel I_\perp)/({}^{y}_\perp I_\perp + {}^{y}_\parallel I_\perp) \qquad (1)
\end{aligned}
$$

where ${}_{m}I_{n}$ is fluorescence intensity, the left and right subscripts denote the orientation relative to the fiber axis of the excitation and emission polarizers, respectively, and the presuperscripts x and y indicate directions of illumination (Fig. 1). ${}^{x}Q_\parallel$ and ${}^{x}Q_\perp$ are identical to the polarization ratios that were previously termed $Q_\parallel$ and $Q_\perp$, respectively (Irving et al., 1995; Allen et al., 1996). ${}^{y}Q_\parallel$ and ${}^{y}Q_\perp$ are introduced here for illumination propagating perpendicular to the observation axis (*y* illumination; see Fig. 1). $D_\parallel$ and $D_\perp$ are the amplitudes of the 84.2-kHz modulation of the polarized components of fluorescence intensity; $L_\parallel$ and $L_\perp$ are corresponding mean intensities of fluorescence (Allen et al., 1996).

$D_\parallel$ and $D_\perp$ were calculated in real time by two lock-in amplifiers (model 3961B; Ithaco, Ithaca, NY), and $L_\parallel$ and $L_\perp$ were obtained by passing the outputs of the two photomultiplier tubes through 1-kHz low-pass filters (model 3100F; Pacific Instruments, Concord, CA) as described in Allen et al. (1996). $Q_\parallel$ and $Q_\perp$ were calculated (using Eq. 1) off-line from the digitized *D* and *L* signals after small background signal levels obtained with the exciting light blocked were subtracted. This procedure provided *Q* signals with 500-μs time resolution. Amplitude scale factors used to calibrate the ${}^{x}Q$ ratios were obtained with an isotropic, immobilized sample of IATR (lot 70241; Research Organics, Cleveland, OH) imbedded in epoxy, for which ${}^{x}Q_\parallel = {}^{x}Q_\perp = 0.46$, determined on an independent, internally calibrated, static polarization microscope, as described by Allen et al. (1996).

${}^{y}D_\perp$ and ${}^{y}Q_\perp$ are zero for isotropic samples (equation 8 of Borejdo and Putnam, 1977), so another fluorescent object with known anisotropic polarization was required to calibrate these two signals. To prepare an anisotropic calibration sample, IATR (Research Organics) was mixed with polyvinyl acetate, dried, and uniformly stretched about fivefold along one axis to introduce an orientation preference of the rhodamine dipoles (van Gurp et al., 1989). A film of this material, ~200 μm thick, was glued between two small glass 45°, 45°, 90° prisms with clear epoxy (type 302; Epoxy Technology, Billerica, MA). The resulting cube, 8 mm on each edge, could be placed at the position of the fiber and illuminated from both *x* and *y* directions. Polarization ratios of ${}^{y}Q_\parallel = 0.300$ and ${}^{y}Q_\perp = 0.205$ were obtained for the cube in the static polarization microscope, and these values were used to calibrate ${}^{y}Q_\parallel$ and ${}^{y}Q_\perp$ in the transient setup.

For improved time resolution, $D_\parallel$, $D_\perp$, $L_\parallel$, and $L_\perp$ were extracted off-line from the modulated parallel and perpendicular fluorescence intensity signals recorded at a sampling rate of 2 μs. The two photomultiplier tube output signals were analyzed separately. A 84.2-kHz sine wave was fitted to the oscillations of polarized fluorescence intensity. The mean values ($L_\parallel$ and $L_\perp$), amplitudes ($D_\parallel$ and $D_\perp$), frequency, and phase of the fitted sine wave were adjusted within successive segments of 25 samples according to a Levenberg-Marquardt algorithm (Press et al., 1992). For a 25-sample segment beginning at the *i*th sample of a trace, the next segment was fitted beginning at the $(i + 14)$th sample, so the fitted segments overlapped by 11 samples. This procedure produced a series of mean values, $L_\parallel$ and $L_\perp$, and amplitudes, $D_\parallel$ and $D_\perp$, for the segments. The time course of each signal, $L_\parallel$, $L_\perp$, $D_\parallel$, and $D_\perp$, was generated from the fitted values by combining data from the overlapping segments according to a set of linearly shifting ratios given by $(j/12:(12 - j)/12)$, where $j = 1, 2, \ldots 11$ is the index within the overlap of the two segments. This procedure amounts to a linearly varying interpolation between the results of fitting the 82.4-kHz sine wave to the two overlapping segments. Each of the series of values obtained for $L_\parallel$, $L_\perp$, $D_\parallel$, and $D_\perp$ was then averaged over successive segments of 25 points, yielding an effective time resolution of 50 μs.

${}^{y}D_\perp$ and ${}^{y}Q_\perp$ were smaller than the other *D* and *Q* signals because of probe disorder. ${}^{y}D_\perp$ was usually too small to be determined reliably by the above procedure, so a different computer algorithm was used for that signal. This procedure emulated a lock-in amplifier and did not require fitting sine functions to the perpendicular fluorescence intensity. A fixed-amplitude reference sine wave was generated from the simultaneously recorded parallel fluorescence intensity with *y* illumination by fitting 25-sample segments overlapped by 11 samples as above. This algorithm automatically corrected for any phase jitter in the photoelastic modulator or sampling clocks. The phase of the fixed-amplitude reference was further shifted (typically by 45°) to cancel a phase difference introduced by the photomultiplier preamplifiers. The perpendicular fluorescence intensity signal was multiplied by the reference sine wave to frequency-shift the 84.2 kHz oscillations to DC and even-order harmonics of 84.2 kHz (Schwartz, 1959, p. 160). Frequency components above 20 kHz were then removed by successively filtering the product trace through 84.2 kHz and 168.4 kHz notch filters (second-order recursive, quality 0.5), a 200-kHz low-pass filter (second-order recursive, quality 0.5), and, finally, a second-order 55-point low-pass Savitzky-Golay (1964) transversal filter. This routine gave the same amplitude and response time as the simpler 25/11-point sine wave fitting method used for the other three *D* signals. Software to automate this sequence of operations was written in-house; further details and C++ source code are available on request.

$Q_\parallel$ and $Q_\perp$ were calculated from the *D* and *L* signals at 50-μs time resolution, using Eq. 1 and calibration scale factors derived from the immobilized samples of IATR as described above for the signals sampled at 500 μs. Although only the 50-μs-resolution signals, available after the signal processing, were used in the figures and analysis presented below, it was useful to have the 500-μs-resolution signals available immediately to evaluate the quality of the recordings and progress of the experiments.

Analysis of fluorescence polarization data

To quantitatively assess changes in the probe orientation, we fit simple models of the orientational distributions to the polarization ratio data. As in earlier work (Ling et al., 1996; Allen et al., 1996; Berger et al., 1996), these models assume that the fluorophores wobble on a time scale that is fast compared with the fluorescence lifetime within a cone of semiangle δ (Irving, 1996). In the previous work we did not evaluate δ directly, but fit models to the orientation distribution, using a range of δ values. Here we introduce a procedure that uses *y* illumination to estimate δ experimentally.

With samples like a muscle fiber that have cylindrical symmetry about the *z* axis, the instantaneous intensities (*I*), modulation amplitudes (*D*), and

mean intensities (L) that have at least one parallel pre- or postsubscript are identical for x and y illumination. Therefore the only fluorescence intensity that differs between x and y illumination is ${}_{\perp}I_{\perp}$. The expressions for ${}^{x}Q_{\parallel}$ and ${}^{y}Q_{\parallel}$ do not contain ${}_{\perp}I_{\perp}$, so ${}^{x}Q_{\parallel}$ and ${}^{y}Q_{\parallel}$ are expected to be equal. Indeed, measured values of these two quantities were always equal within experimental error (see Results). An average of the two, termed $Q_{\parallel}$ with no presuperscript, was used for interpretation of the polarization ratios in terms of orientational distributions. Thus there are three independent polarization ratios: $Q_{\parallel}$, ${}^{x}Q_{\perp}$, and ${}^{y}Q_{\perp}$.

Irving (1996) presented equations for polarized fluorescence intensities from cylindrically symmetrical samples in which probes undergo motions that are rapid compared to the fluorescence lifetime but are restricted to a cone of half-width δ. Assuming that the absorption and emission dipole moments are parallel, the fluorescence intensities are given by

$$ {}^{x}_{\parallel}I_{\parallel} = {}^{y}_{\parallel}I_{\parallel} = \tfrac{1}{4}\cdot k\cdot[\omega + (2-3\omega)\cdot\cos^2\theta]^2 $$

$$ {}^{x}_{\perp}I_{\parallel} = {}^{y}_{\perp}I_{\parallel} = {}^{x}_{\parallel}I_{\perp} = {}^{y}_{\parallel}I_{\perp} = \tfrac{1}{8}\cdot k\cdot[2\omega + (2-3\omega)\cdot\sin^2\theta]\cdot[\omega + (2-3\omega)\cdot\cos^2\theta] $$

$$ {}^{x}_{\perp}I_{\perp} = \tfrac{1}{32}\cdot k\cdot[8\omega^2 + 8\omega\cdot(2-3\omega)\cdot\sin^2\theta + (2-3\omega)^2\cdot 3\sin^4\theta] $$

$$ {}^{y}_{\perp}I_{\perp} = \tfrac{1}{32}\cdot k\cdot[8\omega^2 + 8\omega\cdot(2-3\omega)\cdot\sin^2\theta + (2-3\omega)^2\cdot\sin^4\theta], $$

and

$$ \omega = [1 - \tfrac{1}{3}\cdot(1 + \cos\delta + \cos^2\delta)], \qquad (2) $$

where δ is the half-width of the cone delimiting the fast probe wobble, θ is the angle between the axis of this cone and the fiber axis, and k is an intensity coefficient that depends on the concentration of probes and the optical set-up. The first three equations above were given in slightly different form in Irving (1996), and the fourth equation can be derived by similar calculation. The factor of 3 in the last term of the expression for ${}^{x}_{\perp}I_{\perp}$ compared to that for ${}^{y}_{\perp}I_{\perp}$ causes these two intensities to be independent, giving the extra information required to estimate δ.

The absorption and emission dipoles are assumed to be colinear because the limiting polarization ratio of rhodamine in viscous media is close to 0.5, implying a small angle between the two dipoles (Chen and Bowman, 1965). We obtain polarization ratios for a dilute random, immobilized sample of Rhodamine B (Acros Organics, Springfield, NJ) of nearly 0.490, which would correspond to an angle of less than 8° between the absorption and emission dipoles. Furthermore, in muscle fibers, P ratios (which are related to the orientation of the emission dipoles the same way the Q ratios are related to that of the absorption dipoles) are approximately equal to the corresponding Q ratios (Sabido-David et al., 1998a), implying that the absorption and emission dipoles have the same orientational distribution.

The two orientation distributions used in Ling et al. (1996) and Allen et al. (1996) were used to fit the measured Q ratios. The Gaussian model assumes a single population of probes that has a Gaussian angular distribution, $G[\alpha] = e^{-(\alpha-\theta_g)^2/2\sigma^2}$, with peak angle θ_g and dispersion σ (Allen et al., 1996). The helix plus isotropic model assumes two populations of probes with one fraction, f, that is completely disordered (isotropic) and another fraction, $1 - f$, at an angle θ_h with respect to the fiber axis. This model is similar to one introduced by Tregear and Mendelson (1975). To predict Q ratios for a population of probes with a given distribution of axial angles, θ, the intensities given by Eq. 2 were summed over the distribution and then inserted into the expressions defining the Q ratios (Eq. 1) using routines developed with Mathcad 5.0+ software (Math Soft, Cambridge, MA). When the intensities were summed, the Gaussian distribution was multiplied by a $\sin(\theta)$ weighting factor as in Allen et al. (1996). Note that the factor k in Eq. 2 drops out when Q ratios are calculated, so it does not need to be evaluated.

Each model is described by three parameters, θ_g, σ, and δ, for the Gaussian model and θ_h, f, and δ for the helix plus isotropic model, and could be fit to the three independent polarization ratios ($Q_{\parallel}$, ${}^{x}Q_{\perp}$, and ${}^{y}Q_{\perp}$) by adjusting its three parameters. With the current data set, exact fits that constrained all three adjustable parameters were obtained for both models. The extent of rapid wobble (δ) was found to be the same for both models (see Results). Thus the addition of y illumination to the technique used previously allows δ to be estimated along with two parameters that describe a particular form of the axial orientational distribution.

Sinusoidal changes of fiber length

In some experiments (Figs. 8 and 9), 500-Hz sinusoidal length changes were applied to the fibers. ${}^{x}Q_{\parallel}$ and ${}^{x}Q_{\perp}$ traces, at 50 μs effective sampling rate, were obtained as described above. The imposed sinusoidal length changes caused small sinusoidal deflections of the Q traces. The amplitude and phase of these sinusoidal components were determined using the lock-in amplifier emulation software. Each Q trace was multiplied by a fixed-amplitude 500-Hz reference sine wave generated from the recorded motor trace. Oscillatory components of this product trace were removed by successive filtering through 500-Hz and 1-kHz notch filters (second-order recursive, quality 0.5), a 200-Hz low-pass filter (second-order recursive, quality 0.5), and, finally, the 55-point low-pass Savitzky-Golay (1964) transversal filter. The resulting trace is the amplitude of the 500-Hz oscillatory component of the Q signal in phase with the motor deflection. We define the signals $R_{\perp}$ and $R_{\parallel}$ as the amplitudes of these in-phase oscillatory components in $Q_{\perp}$ and $Q_{\parallel}$, respectively. The procedure was repeated using a fixed-amplitude reference sine wave that had been phase shifted 90° from the motor position signal to calculate the amplitude of the out-of-phase components of the 500-Hz oscillations in the Q signals.

Experimental protocol

Fibers were activated by transfer from relaxing solution via two washes of preactivating solution into activating solution (Table 1). The fiber was incubated in each solution (except activating solution) for at least 2 min. When maximum tension was reached, a shutter in the laser excitation path opened and recording of the fluorescence intensities began, then a sequence of preprogrammed length changes, termed an experimental trial, was applied to the fiber. The sequence was a series of releases and restretches to the original length, all of the same size. Various intervals (1, 2, 4, 8, 16, 32, 64, and 128 ms) between the release and the restretch were programmed into the pulse sequence, and the whole sequence was usually repeated three times during each trial. Corresponding sequences of stretches and rereleases were also applied. At least 200 ms of recovery was allowed each time the fiber was returned to its original length. After each experimental trial in activating solution, the fiber was returned directly to relaxing solution. Each amplitude of length step was applied in one trial with x illumination, one with y illumination, and one for recording striation spacing changes by white light diffraction.

For rigor experiments the fiber was transferred from relaxing solution to 0.1 mM MgATP relaxing solution, then to rigor solution (Table 1). Experimental trials with length changes of various amplitudes and signs and with x illumination, y illumination, and white light diffraction were applied during each episode of rigor without relaxing the muscle fiber between trials.

The order of the measurements varied between experiments. A typical experiment included four amplitudes of length step during active contraction, each measured with the setup in the x illumination, y illumination, and white light diffraction modes, to give a total of 12 active contractions plus one or two periods of rigor. The initial measurements were often repeated at the end of the experiment to check for fiber degradation. Typically, the polarization ratios in rigor deteriorated (became less ordered) during the course of an experiment more than the ratios in active contraction. This point is detailed further in the Results.

For experiments using laser photolysis of caged ATP, fibers were transferred from rigor solution through two washes of a rigor solution containing Ca^{2+}, then into the Ca-rigor solution plus caged ATP (Table 1). Caged ATP was photolyzed by a pulse from a frequency-doubled ruby laser (347 nm) focused onto the fiber through a fused silica window on the side of the measuring trough (same direction as the *y* illumination in Fig. 1; see also Tanner et al., 1992). A single pulse from the laser photoreleased 0.3–1.0 mM ATP, as determined by anion exchange HPLC (Goldman et al., 1984a). Fluorescence signals were recorded during the subsequent development of tension. After steady tension was reached, the fiber was transferred to relaxing solution.

RESULTS

Steady-state polarization ratios

The steady-state fluorescence polarization ratios (Table 2) obtained with *x* illumination from fibers containing RLC labeled on Cys^{108} with 6-IATR (subsequently referred to as $Cys^{108\text{-}6}$) are similar to those reported previously (Irving et al., 1995; Sabido-David et al., 1998a). In rigor, ${}^{x}Q_{\parallel}$ was smaller than ${}^{x}Q_{\perp}$. With *y* illumination, ${}^{y}Q_{\parallel}$ was similar to ${}^{x}Q_{\parallel}$ and ${}^{y}Q_{\perp}$ was positive. ${}^{y}Q_{\parallel}$ and ${}^{x}Q_{\parallel}$ are expected to be equal because of the cylindrical symmetry of the muscle fiber, but ${}^{x}Q_{\perp}$ and ${}^{y}Q_{\perp}$ are independent of each other. These results indicate that the probe dipoles were preferentially oriented perpendicular to the fiber axis. When the Gaussian model was fit to the rigor polarization ratios, the dispersion of the probe angle distribution (σ) was 18.3°, indicating a well-ordered orientational distribution, and in the helix plus isotropic model the fraction, *f*, of disordered probes was 0.42.

During active contraction, the difference between ${}^{x}Q_{\parallel}$ and ${}^{x}Q_{\perp}$ for $Cys^{108\text{-}6}$ was less than in rigor, and ${}^{y}Q_{\perp}$ was closer to zero, indicating that the probe orientations were less perpendicular than in rigor (Table 2). According to the Gaussian model, the dispersion of the orientational distribution increased to 24.7°, and in the helix plus isotropic model, 68% of the probes were disordered. The peak angle of the Gaussian distribution, θ_g, and the angle of the helical fraction, θ_h, were both smaller in active contraction than in rigor. In relaxing solution at 200 mM ionic strength, the *Q* ratios and fitted orientation parameters were similar to those in active contraction.

In low ionic strength (20 mM) relaxing solution at 3°C (Table 1), all of the *Q* ratios for $Cys^{108\text{-}6}$, with the exception of ${}^{y}Q_{\perp}$, were intermediate between those observed in relaxation at 200 mM ionic strength and in rigor. ${}^{x}Q_{\perp}$ in low ionic strength relaxation was consistent with a linear combination of 79% of the polarized fluorescence intensities in rigor and 21% of those in relaxation at 200 mM ionic strength. Likewise, the ${}^{x}Q_{\parallel}$ value obtained in low ionic strength relaxation was consistent with 72% of the intensities in rigor and 28% of those in relaxation. The fitted values of θ_g and θ_h in low ionic strength relaxation were similar to those in rigor, but both models showed an increased dispersion (σ) or disorder (*f*) compared to rigor.

The fluorescence polarization ratios from fibers incorporating the $Cys^{108\text{-}5}$ probe were markedly different from those with $Cys^{108\text{-}6}$. The *Q* ratios changed very little among rigor, active contraction, and relaxation. ${}^{x}Q_{\parallel}$ and ${}^{y}Q_{\parallel}$ were slightly smaller than ${}^{x}Q_{\perp}$ in active contraction and relaxation. ${}^{y}Q_{\perp}$ was slightly negative in all three states. Both orientation models suggested that the $Cys^{108\text{-}5}$ probes were less ordered and more parallel to the fiber axis than the $Cys^{108\text{-}6}$ probes.

The mean values of ${}^{x}Q_{\parallel}$ and ${}^{x}Q_{\perp}$ for $Cys^{108\text{-}5}$ in Table 2 are different from those reported by Sabido-David et al. (1998a), particularly in rigor. Those authors found a significant axial preference (${}^{x}Q_{\parallel} > {}^{x}Q_{\perp}$) in rigor, whereas the results in Table 2 show virtually no difference between ${}^{x}Q_{\parallel}$ and ${}^{x}Q_{\perp}$ in rigor. This discrepancy is related to the order in which the measurements were made. Four of the $Cys^{108\text{-}5}$ fibers in Table 2 were put into rigor after a series of eight active contractions. These four fibers showed a slight perpendicular preference in rigor, with average values of ${}^{x}Q_{\parallel}$ and ${}^{x}Q_{\perp} = 0.322$ and 0.358, respectively. The other two

TABLE 2 Steady-state polarization ratios and fitted parameters of two different orientation distributions

	$Cys^{108\text{-}6}$				$Cys^{108\text{-}5}$		
	Rigor	Active	Relaxed	Low ionic strength	Rigor	Active	Relaxed
${}^{x}Q_{\parallel} \pm$ SEM	0.144 ± 0.014	0.286 ± 0.028	0.304 ± 0.032	0.197 ± 0.026	0.340 ± 0.036	0.322 ± 0.011	0.318 ± 0.037
${}^{y}Q_{\parallel} \pm$ SEM	0.151 ± 0.036	0.291 ± 0.018	0.305 ± 0.019	0.202 ± 0.039	0.338 ± 0.042	0.327 ± 0.020	0.306 ± 0.072
${}^{x}Q_{\perp} \pm$ SEM	0.486 ± 0.012	0.425 ± 0.019	0.430 ± 0.018	0.476 ± 0.006	0.341 ± 0.026	0.375 ± 0.005	0.364 ± 0.005
${}^{y}Q_{\perp} \pm$ SEM	0.060 ± 0.017	0.003 ± 0.006	0.007 ± 0.005	0.064 ± 0.005	−0.047 ± 0.007	−0.012 ± 0.014	−0.035 ± 0.010
n_x	4	16	16	2	6	6	6
n_y	5	5	5	2	6	6	6
σ	18.3 ± 0.4	24.7 ± 1.1	25.6 ± 1.1	22.3 ± 1.4	32.6 ± 11.3	31.9 ± 6.7	27.2 ± 4.2
θ_g	60.6 ± 0.7	54.3 ± 0.7	54.1 ± 0.8	59.7 ± 0.8	41.4 ± 13.5	47.8 ± 3.8	49.3 ± 2.9
δ	18.2 ± 0.4	22.0 ± 1.6	21.1 ± 1.5	20.6 ± 0.3	25.6 ± 2.7	25.4 ± 1.5	24.2 ± 1.2
f	0.42 ± 0.02	0.68 ± 0.03	0.70 ± 0.03	0.52 ± 0.04	0.90 ± 0.18	0.83 ± 0.05	0.80 ± 0.09
θ_h	65.0 ± 0.5	62.6 ± 0.4	63.1 ± 0.3	65.9 ± 0.0	62.2 ± 8.8	60.7 ± 2.1	57.1 ± 1.2

θ_g and σ are the peak angle and dispersion in the Gaussian model; θ_h is the angle of the ordered fraction of probes and *f* is the fraction of isotropic probes in the helix plus isotropic model. In both models δ is the half-width of a cone delimiting probe wobble faster than the decay time of the fluorescence excited state. θ_g, θ_h, σ, and δ are given in degrees. n_x and n_y are the numbers of fibers used for *x* illumination and *y* illumination measurements, respectively. Model parameters were fitted from an average of ${}^{x}Q_{\parallel}$ and ${}^{y}Q_{\parallel}$. Model parameters were fitted to data from individual fibers and then averaged.

fibers in Table 2 were measured in rigor at the start of the experiments and showed an axial preference, with average values of ${}^{x}Q_{\parallel}$ and ${}^{x}Q_{\perp}$ of 0.379 and 0.308, similar to the values reported by Sabido-David et al. (1998a). After a series of 12 active contractions for fluorescence polarization and sarcomere length measurements, the rigor fluorescence polarization measurements were repeated in these two fibers. The axial preference in rigor observed at the start of the experiment had decreased, so that the Q ratios were similar to those in the four fibers that had been put into rigor only at the end of the experiments. The changes in the rigor Q ratios associated with fiber rundown led to large changes in the fitted model parameters, as can be seen by the large standard errors in Table 2 for θ_g, σ, θ_h, and f for Cys$^{108\text{-}5}$. Because the Q transients induced by length changes, which are presented below, were not appreciably affected by fiber rundown, we did not pursue the mechanism of this effect further.

The half-width of the cone in which the probes move freely on a time scale faster than the fluorescence lifetime (δ) was 18°–22° for Cys$^{108\text{-}6}$ and 24°–26° for Cys$^{108\text{-}5}$. In all of the conditions studied, the value of δ obtained with the Gaussian model was identical to that obtained with the helix plus isotropic model. Therefore the estimate of δ does not depend on the specific form of the probe orientational distribution (see also Dale et al., 1997). For both probes, δ did not depend on the physiological state of the muscle, suggesting that the extent of wobble is determined by the local interaction of the probes with the RLC, rather than the angular distribution of the RLCs themselves.

Q transients produced by length steps in active contraction

Rapid length steps applied in active contraction partly synchronize the motions of attached cross-bridges. Fluorescence polarization has been used previously to detect changes in the orientation of RLC probes during these motions (Irving et al., 1995). Here we measured transients of the four polarization ratios (${}^{x}Q_{\parallel}$, ${}^{y}Q_{\parallel}$, ${}^{x}Q_{\perp}$, and ${}^{y}Q_{\perp}$) produced by step releases and stretches for both Cys$^{108\text{-}6}$ and Cys$^{108\text{-}5}$. For Cys$^{108\text{-}6}$ in active contraction, the Q ratios showed deflections both during and after the imposed shortening step (Fig. 2), as reported previously (Irving et al., 1995). A shortening step produced an increase in ${}^{x}Q_{\perp}$ and a decrease in both $Q_{\parallel}$ signals (Fig. 2 *A*), indicating tilting of the Cys$^{108\text{-}6}$ dipole away from the fiber axis. For releases, the deflections of the $Q_{\parallel}$ traces were consistently smaller than those of the $Q_{\perp}$ traces. Step stretches caused deflections of all four Q ratios in the direction opposite that of releases (Fig. 2 *B*), as reported previously for *x* illumination (Irving et al., 1995). In the fiber in Fig. 2, the sarcomere length continued to change after the step was completed, presumably because of length changes in compliant regions at the ends of the fiber. However, the component of the Q transient that occurs after the length step is not due to this delayed change in sarcomere length; it was still present in fibers in which the delayed sarcomere length change was negligible (e.g., see Fig. 4 below, and Irving et al., 1995).

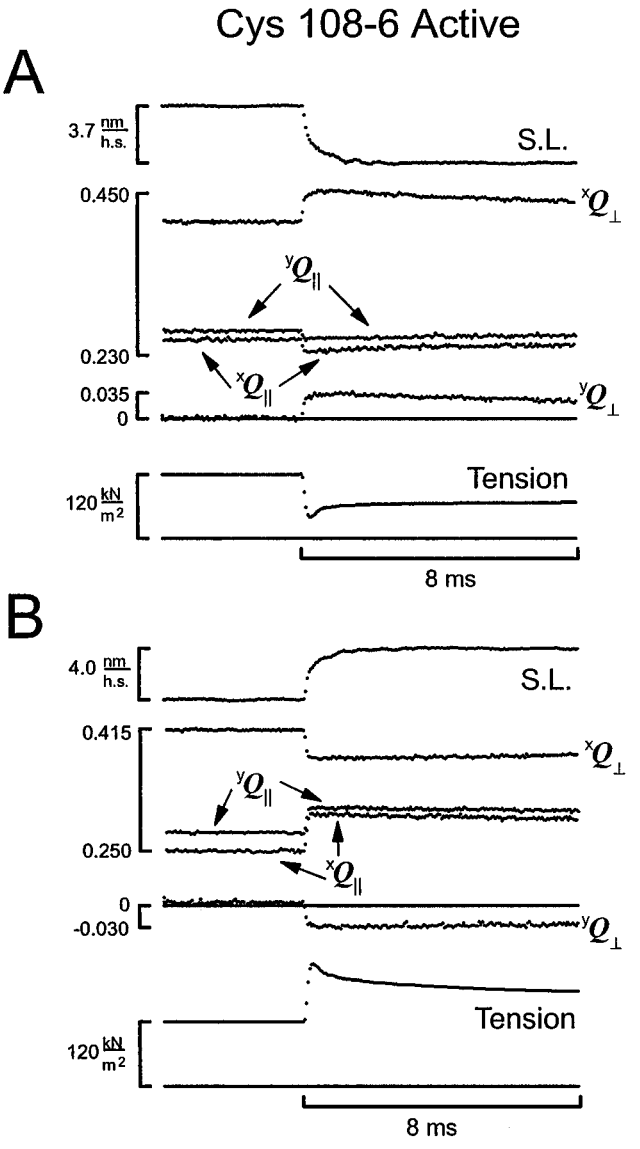

FIGURE 2 Transients of sarcomere length (S.L.), polarization ratios (Q), and tension produced by a release (*A*) and stretch (*B*) in active contraction for a fiber exchanged with Cys$^{108\text{-}6}$-labeled RLC. The four fluorescence polarization ratios ${}^{x}Q_{\parallel}$, ${}^{x}Q_{\perp}$, ${}^{y}Q_{\parallel}$, and ${}^{y}Q_{\perp}$ are defined in Materials and Methods. In each panel, the horizontal line below the tension trace is the tension baseline recorded in relaxing solution. The horizontal line for ${}^{y}Q_{\perp}$ indicates zero polarization ratio. All traces are the average response from 15 length steps in a single activation. The *x* illumination, *y* illumination Q ratios and sarcomere length (S.L.) signals were recorded in separate activations. Relaxed sarcomere length, 2.72 μm; fiber length, 1.97 mm; cross-sectional area, 3896 μm^2.

Q transients for *y* illumination have not been reported previously. For Cys$^{108\text{-}6}$, the changes in ${}^{y}Q_{\parallel}$ were similar to those in ${}^{x}Q_{\parallel}$ in both amplitude and time course. The slight differences observed between ${}^{y}Q_{\parallel}$ and ${}^{x}Q_{\parallel}$ (Fig. 2) are probably due to their being recorded in separate activations. The steady-state value of ${}^{y}Q_{\perp}$ for Cys$^{108\text{-}6}$ during active

contraction was close to zero (the initial value in Fig. 2 is similar to the steady-state value in Table 2). A quick release caused an abrupt positive deflection of ${}^{y}Q_{\perp}$ followed by a further change in the same direction during quick tension recovery (Fig. 2 *A*), consistent with the probes tilting away from the muscle fiber axis. The amplitude and time course of the ${}^{y}Q_{\perp}$ transients were similar to those of ${}^{x}Q_{\perp}$, even though their static values were so different (Fig. 2). This similarity between the ${}^{x}Q_{\perp}$ and ${}^{y}Q_{\perp}$ transients was observed in all experiments, with both $Cys^{108\text{-}6}$ and $Cys^{108\text{-}5}$, for stretches and releases, and in rigor and in activation. This behavior is expected for deflections of θ_g in the Gaussian model during a length step, given the range of initial angles observed in the present experiments.

For fibers containing the $Cys^{108\text{-}5}$ probe, the *Q* transients produced by length steps (Fig. 3; note the expanded *Q* ratio scale) were much smaller than for $Cys^{108\text{-}6}$ (Fig. 2). For $Cys^{108\text{-}5}$, step releases caused ${}^{x}Q_{\perp}$ and ${}^{y}Q_{\perp}$ to decrease and ${}^{x}Q_{\parallel}$ and ${}^{y}Q_{\parallel}$ to increase slightly during the length steps (Fig. 3 *A*). The directions of these small changes were reproducible. Stretches deflected the *Q* ratios in the same direction as releases, but the main change produced by stretches took place after the length steps were complete. In some fibers a stretch produced a slight increase in ${}^{x}Q_{\parallel}$ and ${}^{y}Q_{\parallel}$; in other fibers ${}^{x}Q_{\parallel}$ and ${}^{y}Q_{\parallel}$ were constant, as in Fig. 3 *B*.

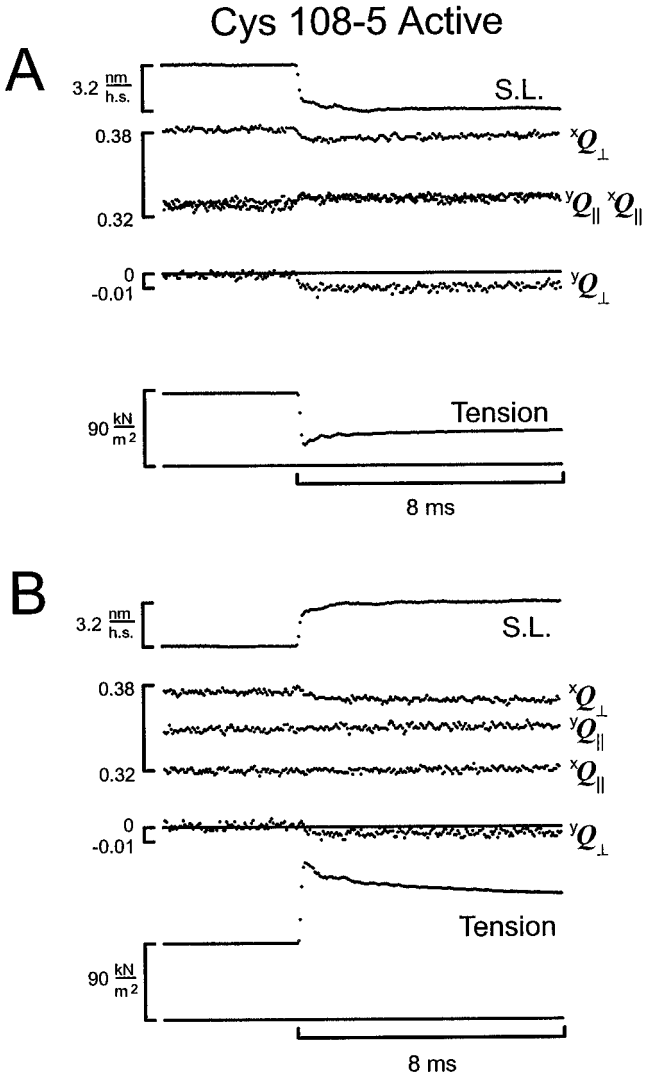

FIGURE 3 Transients of sarcomere length (S.L.), four polarization ratios (*Q*), and tension, produced by a release (*A*) and stretch (*B*) in active contraction for a fiber exchanged with $Cys^{108\text{-}5}$-labeled RLC. Recording protocol and baselines are as in Fig. 2, except that the scale for the *Q* ratios has been expanded. Relaxed sarcomere length, 2.48 μm; fiber length, 3.03 mm; cross-sectional area, 10,183 μm^2.

Dependence of the *Q* transients on the size of applied length steps

Stretches of up to 7 nm/h.s. and releases of up to 12 nm/h.s. were applied to actively contracting fibers containing $Cys^{108\text{-}6}$. The resulting transients in ${}^{x}Q_{\parallel}$ and ${}^{x}Q_{\perp}$ for a typical fiber are shown in Fig. 4. Stretches of three different amplitudes caused negative deflections of ${}^{x}Q_{\perp}$ and positive deflections of ${}^{x}Q_{\parallel}$. The deflections of ${}^{x}Q_{\parallel}$ produced by stretches were somewhat larger than those of ${}^{x}Q_{\perp}$. Releases of four different amplitudes caused deflections in the opposite direction. In this case the ${}^{x}Q_{\perp}$ changes were larger than those of ${}^{x}Q_{\parallel}$.

For length steps of 2–4 nm/h.s., tension quickly recovered toward its isometric value, but ${}^{x}Q_{\perp}$ continued to change during tension recovery in the same direction as during the length step itself (releases labeled 1 and 2 in the *inset* of Fig. 4 *A*). However, a release of 12 nm/h.s. (*trace 4* in Fig. 4 *A*) caused a smaller deflection of ${}^{x}Q_{\perp}$ than a release of 7 nm/h.s. (*trace 3*). This behavior was not due to fiber rundown in successive contractions. Very little sarcomere shortening took place during the quick recovery in this fiber (Fig. 4 *C*).

${}^{x}Q_{\parallel}$ transients for releases were smaller than those for stretches. The quick recovery after a release was in the direction opposite that of the elastic response. As with ${}^{x}Q_{\perp}$, the largest release (12 nm/h.s.) caused a smaller deflection of ${}^{x}Q_{\parallel}$ than a release of 7 nm/h.s. By ~5 ms after the step, ${}^{x}Q_{\parallel}$ for the 12-nm/h.s. release had recovered substantially toward its isometric value (Fig. 4 *A*).

The amplitudes of each tension and *Q* transient were measured at the end of the length step (at the time of the peak tension response; *filled symbols* in Fig. 5) and are here termed the "elastic" components of the transients. We also measured the value of each tension and *Q* transient after four time constants of an exponential decay that was fitted, with the addition of a linear decay term, to 8 ms of the tension trace after the step. The time constants ranged from ~1.6 ms for releases to ~2.7 ms for stretches. The period of four time constants after the step is termed the "quick recovery" of the transients, and the values measured at the end of the quick recovery are shown by open symbols in Fig. 5. Quick tension recovery was less complete here than observed previously in psoas fibers (e.g., Martyn and Chase, 1995). This difference may be due to the presence of the

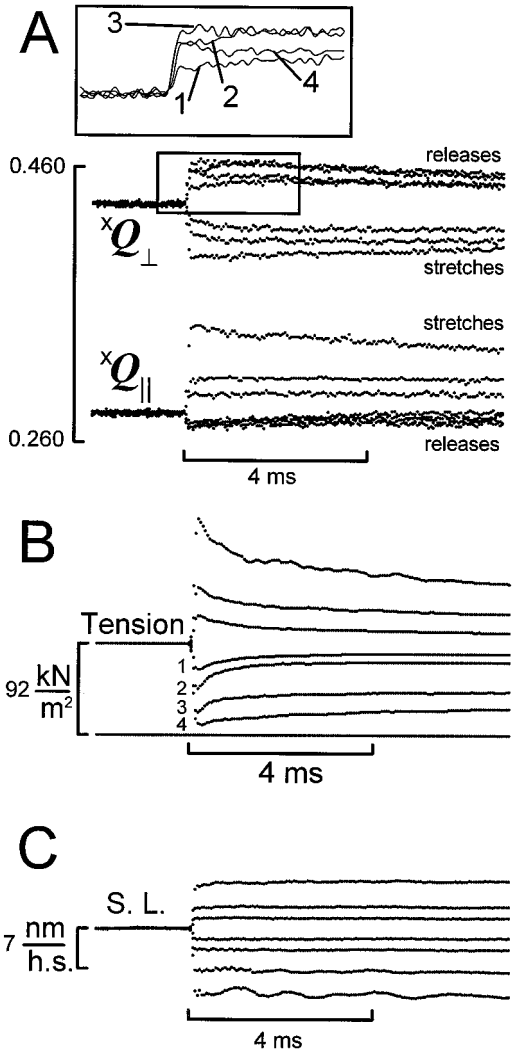

FIGURE 4 Transients in *x* illumination polarization ratios (*Q*) (*A*), tension (*B*), and sarcomere length (S.L.) (*C*) for a range of step sizes in active contraction for a fiber exchanged with $Cys^{108\text{-}6}$-labeled RLC. Each trace is the average of the response to 15 length steps in a single activation. The *Q* and tension transients for each length step amplitude were scaled to superimpose the values before the length step; the sarcomere length traces were shifted vertically to superimpose them before the length step. Three sizes of stretch, ~2, 4, and 7 nm/h.s., and four sizes of release, ~2, 4, 7, and 12 nm/h.s., were applied. The inset shows the initial part of the $^{x}Q_{\perp}$ response for the four releases, numbered to identify them with the corresponding tension traces. In the inset traces, the experimental points have been interpolated using a cubic spline routine. Relaxed sarcomere length, 2.48 μm; fiber length, 3.5 mm; cross-sectional area, 6004 μm^2.

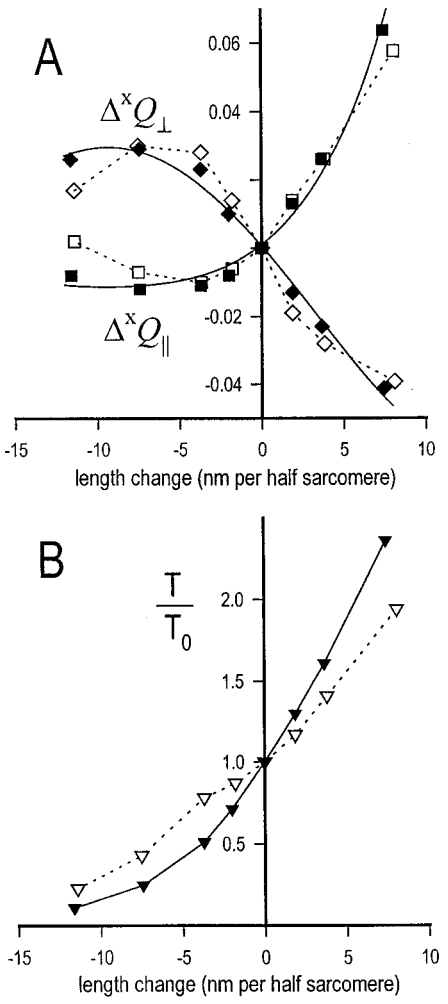

FIGURE 5 Amplitudes of $^{x}Q_{\parallel}$ and $^{x}Q_{\perp}$ transients (*A*) and tension (*B*), in active contraction plotted against the size of the length step. Filled symbols represent the deflections at the end of the length step (the elastic response). Open symbols represent the deflections after the quick recovery in tension (see Results). Squares and diamonds represent the deflections of $^{x}Q_{\parallel}$ and $^{x}Q_{\perp}$, respectively. The smooth curve is calculated from a model presented in the Discussion. Tension (T/T_0) was normalized to the isometric tension before the length step (T_0). The sarcomere length change was measured at the same time point as the *Q* and the tension measurements. Data are from the same fiber as in Fig. 4.

labeled RLC, an effect of the exchange protocol or the large number of contractions and length steps used to record the full set of polarization transients.

For length steps of 2 or 4 nm/h.s., the deflections in $^{x}Q_{\perp}$ produced by stretches and releases were the same size, but in the opposite direction. Two types of nonlinear dependence of the *Q* transients on step amplitude were apparent. As mentioned, $^{x}Q_{\parallel}$ transients for releases were smaller than those for stretches of the same size (Figs. 2, 4, and 5). For stretches of 6–7 nm/h.s., the deflections of $^{x}Q_{\perp}$ and $^{x}Q_{\parallel}$ were -0.034 ± 0.004 and $+0.040 \pm 0.009$, respectively (means $\pm$ SD, $n = 5$ fibers). For releases of the same amplitude, the deflections of $^{x}Q_{\perp}$ and $^{x}Q_{\parallel}$ were $+0.032 \pm 0.008$ and -0.009 ± 0.005, respectively (seven fibers). The amplitude of the *Q* deflections increased with the size of the stretch, but in contrast, the sizes of both $^{x}Q_{\perp}$ and $^{x}Q_{\parallel}$ deflections showed a clear saturation for releases beyond ~5 nm/h.s. The markedly nonlinear saturating responses of the fluorescence polarization ratios to length changes can be explained in terms of the probe dipoles approaching and crossing the plane perpendicular to the fiber axis (the 90° plane) during moderate size releases. The smooth line drawn through the elastic response data in Fig. 5 *A* shows the *Q* deflections expected for a simple geometrical model,

presented in the Discussion, that assumes a fraction of probes cross the 90° plane for the larger releases.

Fitting model orientation distributions to the *Q* deflections

From the $Q_{\parallel}$, ${}^{x}Q_{\perp}$, and ${}^{y}Q_{\perp}$ transients, the Gaussian model was used to estimate changes in θ_g, σ, and δ for the entire population of probes considered as one Gaussian distribution (see Materials and Methods). Under this (probably unrealistic) assumption, the estimated half-width of the cone delimiting the rapid probe wobble (δ) changed slightly ($+1°$ for a 3 nm/h.s. stretch and $-1°$ for a 3 nm/h.s. release). As expected from the positive deflections of ${}^{x}Q_{\perp}$ and ${}^{y}Q_{\perp}$, the peak angle of the Gaussian distribution (θ_g) became more perpendicular to the fiber axis after a release. The opposite behavior was observed after a stretch. The maximum change, $\Delta\theta_g$, was about $-6°$ for the 7 nm/h.s. stretch. A plot of $\Delta\theta_g$ versus length step amplitude (not shown) had a nonlinear shape similar to that of the $\Delta{}^{x}Q_{\perp}$ plot in Fig. 5 *A*. The length steps increased the Gaussian dispersion (σ) for all step sizes, except the smallest stretches (2 and 4 nm/h.s.).

Q transients produced by length steps in rigor and low ionic strength relaxing solution

In rigor, the deflections of the *Q* signals were confined to the duration of the applied length changes, consistent with tilting of the probes in a pure elastic response. $Cys^{108\text{-}6}$ and $Cys^{108\text{-}5}$ showed similar *Q* deflections during step stretches (Fig. 6), even though the prestep values were different. For both probes, ${}^{x}Q_{\perp}$ and ${}^{y}Q_{\perp}$ increased, whereas ${}^{x}Q_{\parallel}$ and ${}^{y}Q_{\parallel}$ decreased. ${}^{y}Q_{\perp}$ for $Cys^{108\text{-}6}$ was positive before the step and increased during a stretch; ${}^{y}Q_{\perp}$ for $Cys^{108\text{-}5}$ was negative before the step and became less negative during a stretch. Thus rigor stretches tilted both probes away from the fiber axis.

The stretch response of $Cys^{108\text{-}6}$ in rigor was opposite that in active contraction, as reported previously (Irving et al., 1995). When the size of the length step was varied between releases of ~0.5 nm/h.s. and stretches of 2 nm/h.s., the amplitudes of the *Q* transients were approximately proportional to the size of the length step (not shown), in contrast to the markedly nonlinear amplitude of the active step response (Figs. 4 and 5). The values of $\Delta\theta_g$ and $\Delta\theta_h$ for $Cys^{108\text{-}6}$ in rigor were $1.1° \pm 0.1°$ and $1.1° \pm 0.2°$, respectively (means ± SEM, $n = 3$ fibers) for stretches of ~2 nm/h.s. The value of σ increased, whereas the value of f decreased. $\Delta\theta_g$ and $\Delta\theta_h$ for $Cys^{108\text{-}5}$ in rigor were $2.0° \pm 1.0°$ and $2.0° \pm 1.0°$, respectively (means ± SEM, $n = 5$) for stretches of ~2 nm/h.s.; the change in σ was not reproducible, but f consistently decreased.

Q transients in response to length steps were also measured in low ionic strength relaxing solution (20 mM) at 3°C (Table 1), a condition in which many cross-bridges attach to actin without generating force. Although the static orientation distribution of $Cys^{108\text{-}6}$ dipoles in this condition was close to that in rigor (see Table 2), ${}^{x}Q_{\parallel}$ and ${}^{y}Q_{\parallel}$ increased in response to a stretch of 7 nm/h.s. (Fig. 7), which was the opposite of their transient behavior in rigor (Fig. 6 *A*). The ${}^{x}Q_{\perp}$ and ${}^{y}Q_{\perp}$ signals showed only very small deflections in low ionic strength relaxing solution. These results suggest that the effect of stretch on attached cross-bridges in these conditions is to tilt the $Cys^{108\text{-}6}$ dipoles toward the fiber axis, the same direction as in active contraction. The amplitude of the tilt, estimated as $\Delta\theta_g$ and $\Delta\theta_h$, was ~0.2°. Stretches caused a small increase in both σ and f corresponding to increased disorder of the orientational distribution.

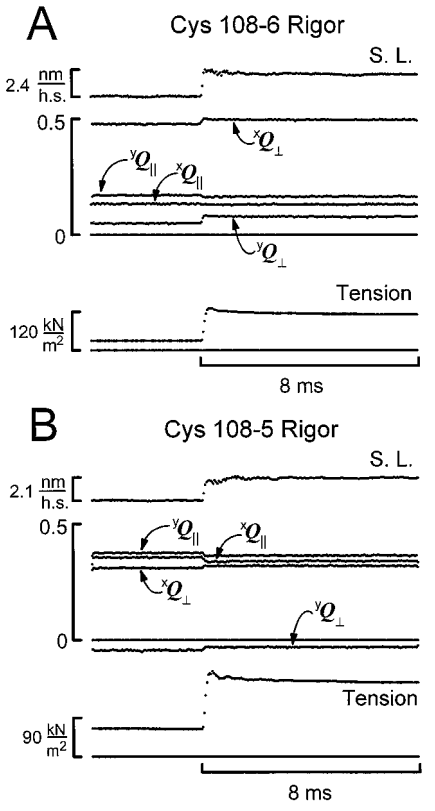

FIGURE 6 Transients of sarcomere length (S.L.), fluorescence polarization ratios (*Q*), and tension, produced by step stretches in rigor, for fibers exchanged with $Cys^{108\text{-}6}$-labeled RLC (*A*), or $Cys^{108\text{-}5}$-labeled RLC (*B*). Zero *Q* and the relaxed tension baseline are indicated by horizontal lines. The calibration bracket for tension is the active isometric tension for each fiber. Each trace is the average of responses to 15 length steps. The *x* illumination, *y* illumination, and sarcomere length (S.L.) signals were recorded during a single rigor contraction in separate experimental trials (see Materials and Methods). Fiber dimensions: (*A*) sarcomere length, 2.72 μm; fiber length, 1.97 mm; cross-sectional area, 3896 μm^2; (*B*) sarcomere length, 2.48 μm; fiber length, 2.13 mm; cross-sectional area, 7965 μm^2.

Stretch response of *Q* signals during activation by photolysis of caged ATP

Step stretches in rigor tilt the $Cys^{108\text{-}6}$ dipoles away from the fiber axis, whereas step stretches in active contraction tilt

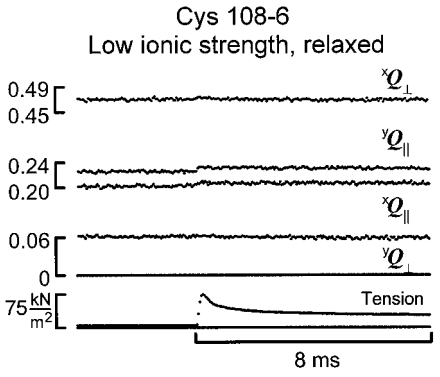

FIGURE 7 Transients of polarization ratios (Q) and tension produced by a step stretch of 7 nm/h.s. in 20 mM ionic strength relaxing solution for a fiber exchanged with $Cys^{108\text{-}6}$-labeled RLC. Zero Q and the relaxed tension baseline at 200 mM ionic strength are indicated by horizontal lines. Sarcomere length, 2.72 μm; fiber length, 1.97 mm; cross-sectional area, 3896 μm^2; $T = 3.2$°C.

them toward it (Figs. 2 and 6; and Irving et al., 1995). This difference in stretch response suggests that the dipoles undergo a large angle change between rigor and active contraction. We studied the kinetics of this angle change by photolyzing caged ATP in fibers containing $Cys^{108\text{-}6}$ RLC while applying sinusoidal length changes to monitor the characteristics of the stretch response. Fig. 8 shows an experiment in which a fiber in rigor was switched to active contraction by photorelease of ~1 mM ATP from caged ATP at ~30 μM free Ca^{2+}. When ATP was released

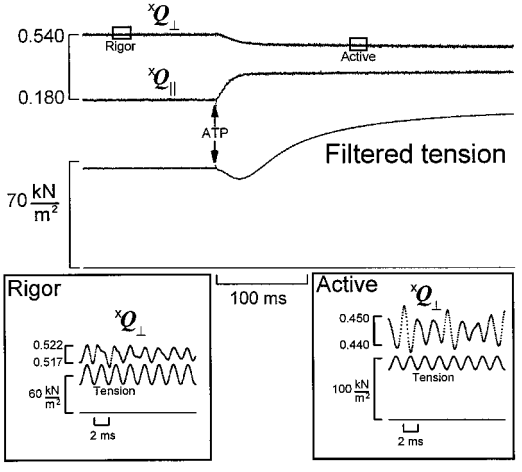

FIGURE 8 Transients of x illumination fluorescence polarization ratios and tension, during activation by photorelease of 1.0 mM ATP from caged ATP (*arrow*) in the presence of ~30 μM free Ca^{2+} $Cys^{108\text{-}6}$. Sinusoidal length oscillations (500 Hz; peak-to-peak amplitude 6 μm) were imposed continuously during the photolysis transient. The resulting oscillations in tension were removed by a software notch filter (second order, quality 0.5). The expanded insets show oscillations of ${}^{x}Q_{\perp}$ and (unfiltered) tension for the short periods of rigor and active contraction indicated by the rectangles in the top trace. The inset polarization traces have been passed through a software 500-Hz band-pass filter (second order, quality 0.5) to reduce out-of-band noise. Sarcomere length, 2.58 μm; fiber length, 2.09 mm; cross-sectional area, 4386 μm^2.

(*arrows*), tension initially declined and then increased to its steady active value. ${}^{x}Q_{\perp}$ decreased and ${}^{x}Q_{\parallel}$ increased promptly during the tension dip, but the Q signals hardly changed during the later development of active tension, as reported by Allen et al. (1996).

A 500-Hz sinusoidal length change (~2 nm/h.s. peak-to-peak) was applied continuously during the photolysis transient. The resulting sinusoidal oscillations of tension were removed by a notch filter. The length changes also induced small oscillations in the Q signals, and traces of ${}^{x}Q_{\perp}$, with random noise reduced by a narrow 500-Hz band-pass filter, are shown in the insets in Fig. 8. The oscillations in ${}^{x}Q_{\perp}$ were approximately in phase with tension in rigor, and ~180° out of phase during active contraction. This phase change is expected from the opposite stretch response in these two states.

We determined the sign and amplitude of the ${}^{x}Q_{\perp}$ oscillations continuously, using software that emulates a lock-in amplifier, as described in Materials and Methods. The resulting signal, $R_{\perp}$, is defined as the amplitude (one-half of the peak-to-peak deflection) of the oscillatory component of ${}^{x}Q_{\perp}$ that is in phase with the length oscillations applied to the fiber. When $R_{\perp}$ is positive, ${}^{x}Q_{\perp}$ increases with imposed stretches (rigor stretch response); when $R_{\perp}$ is negative, ${}^{x}Q_{\perp}$ decreases with imposed stretches (active stretch response). $R_{\perp}$ is zero in relaxed fibers because only attached cross-bridges that tilt in response to length changes contribute to the $R_{\perp}$ signal.

$R_{\perp}$ was 0.0072 ± 0.0022 (mean $\pm$ SEM, $n = 7$) in rigor and -0.0097 ± 0.0032 in active contraction (mean $\pm$ SEM, $n = 7$). When ATP was photoreleased in the muscle fiber, $R_{\perp}$ changed from its positive value in rigor to a negative value characteristic of active contraction. The time course of the change in $R_{\perp}$ (Fig. 9) was intermediate between the faster change in the Q signals and the slower rise in active tension (${}^{x}Q_{\perp}$ is shown in Fig. 9, and both Q signals are shown in Fig. 8). The time course of all three signals (tension, ${}^{x}Q_{\perp}$, and $R_{\perp}$) depended on the amount of ATP released (Fig. 9).

The rapid change of ${}^{x}Q_{\parallel}$ and ${}^{x}Q_{\perp}$ toward their active values reflects early processes of cross-bridge detachment and reattachment triggered by ATP binding to the active site of myosin (Allen et al., 1996), whereas $R_{\perp}$ reflects the stretch response of attached cross-bridges. The intermediate time course of $R_{\perp}$ and its constant level during force development suggest that cross-bridges attach to thin filaments with the active stretch response significantly in advance of force generation. To make this interpretation quantitative, we used the following model of the sequence of cross-bridge states, including a pre-force attached state:

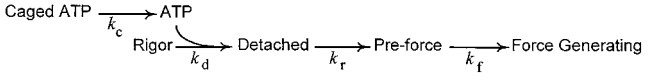

Scheme 1

Values for tension, ${}^{x}Q_{\perp}$, and $R_{\perp}$ were assigned to each state. In rigor, tension, ${}^{x}Q_{\perp}$ and $R_{\perp}$ were set to their values

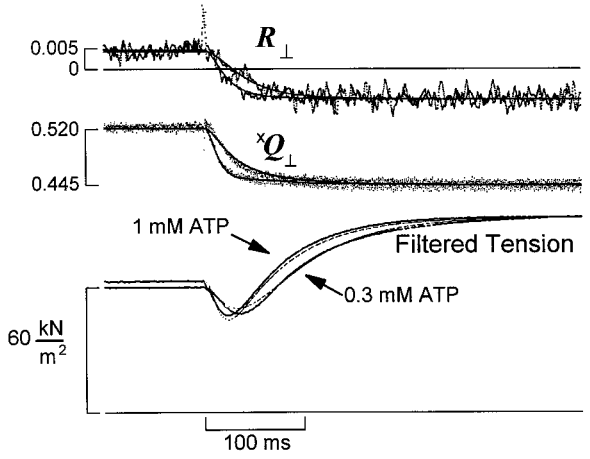

FIGURE 9 In-phase amplitude ($R_\perp$) of 500-Hz oscillations of the $^xQ_\perp$ signal, $^xQ_\perp$, and tension during activation by photorelease of 0.3 mM and 1.0 mM ATP from caged ATP. The slower transients of $R_\perp$, $^xQ_\perp$, and tension are associated with the lower concentration of photoreleased ATP. The solid lines through the $R_\perp$ and $^xQ_\perp$ transients and the dashed lines near the tension transients are the predictions from a kinetic model (Scheme 1 of text) fitted to the data. Horizontal lines indicate zero $R_\perp$ and baseline tension measured in relaxing solution. Data are from the same fiber as in Fig. 8.

before photolysis and in active contraction to their values at the plateau of steady tension. Detached cross-bridges were assigned zero force, zero $R_\perp$, and the active value for $^xQ_\perp$. Preforce cross-bridges were assigned the same values of $^xQ_\perp$ and $R_\perp$ as force-generating cross-bridges, but zero force. With these simple assumptions, values for the rate constants in Scheme 1 of $k_c = 50\ s^{-1}$ at 10°C (Barabás and Keszthelyi, 1984), $k_d = 2.6 \times 10^5\ M^{-1}s^{-1}$ (consistent with Allen et al., 1996), $k_r = 64\ s^{-1}$, and $k_f = 17\ s^{-1}$ provided good fits to the data at both ATP concentrations tested (Fig. 9). Thus the slowing of all of the traces as the ATP concentration was reduced is adequately explained by slower ATP binding.

Phase shifts between the sinusoidal oscillations of the various signals are another indicator of the difference between active and rigor cross-bridges. The tension oscillations in rigor led the imposed length oscillations by 2.2° ± 0.8° (mean ± SEM, $n = 7$), whereas the tension oscillations in active contraction led the length oscillations by 14.2° ± 2.0°. The phase difference between the rigor and active tension oscillations was 12.0° ± 1.5°. These values are similar to those reported before (Goldman et al., 1984b). The $^xQ_\perp$ oscillations led the imposed length changes by 5.9° ± 3.9° (mean ± SEM, $n = 7$) in rigor and by 172.8° ± 2.5° in active contraction. These values are not 180° apart (the phase difference was 167° ± 6°). In active contraction, the peaks of the $^xQ_\perp$ oscillations lagged behind the troughs of the length oscillations by 7.2° ± 2.5° and lagged the troughs of the tension oscillations by 21.5° ± 3.8°. A phase lag in $^xQ_\perp$ is expected for active contraction because of the quick recovery component of the length step response, during which $^xQ_\perp$ changes in the same direction as during the elastic component (see the *inset* of Fig. 4 *A* for small length changes). This phase lag is characteristic of active contraction, but not of rigor.

The amplitude of the $^xQ_\parallel$ oscillations in rigor was too small (0.0010 ± 0.0005, mean ± SEM, $n = 7$) for reliable determination of phase. In active contraction, however, the amplitude of the oscillations in $^xQ_\parallel$ was larger (0.0080 ± 0.0033, with phase offset 0.0° ± 1.1°). The $^xQ_\parallel$ oscillations lagged 14.2° ± 2.3° behind the tension oscillations. The negligible phase shift between $^xQ_\parallel$ and length oscillations in active contraction is consistent with the very small amplitude of the quick recovery component of $^xQ_\parallel$ in the length step transients (Figs. 4 and 5).

In rigor the oscillations of the peak axial angle, θ_g, and the dispersion, σ, in the Gaussian model were virtually in phase with the length change, and both had a peak amplitude of 0.6°. In active contraction the in-phase oscillations of θ_g and σ had peak amplitudes −1.0° and −0.4°, respectively. The active 90° out-of-phase oscillations of θ_g and σ had peak amplitudes of 0.04° and 0.2°, respectively. These 90° out-of-phase components of θ_g and σ that are present in active contraction but not in rigor indicate active motions of the cross-bridge that change the orientational distribution of the light chain region of the myosin head.

DISCUSSION

Fluorescence polarization measurements show that rhodamine probes bound to the regulatory light chains of myosin in muscle fibers tilt in response to quick length changes during active contraction and in rigor. The ratiometric nature of the *Q* polarization ratios described here makes them very insensitive to movement artifacts or changes in fluorescence intensity. The measured *Q* ratios are independent of translation of the probes along the fiber axis, or slewing around that axis. Thus the *Q* ratios depend only on the angle of the probe absorption and emission transition dipoles with respect to the fiber axis.

The transient changes in probe orientation and the differences in orientational distribution between states of relaxation, rigor, and active isometric contraction presented here and in the accompanying paper (Sabido-David et al., 1998a) provide strong evidence for tilting motions of the myosin light chain region during force generation. Similar measurements on muscle fibers labeled at the reactive cysteine of the myosin heavy chain (SH-1, Cys^{707}) do not show tilting in response to length changes (Berger et al., 1996), suggesting that the myosin head contains an internal hinge, probably between the nucleotide-binding domain and the light chain region. Motions around this hinge may underlie force generation. Burghardt et al. (1997) did observe very small deflections of $^xQ_\perp$ and $^xQ_\parallel$ when length changes were applied to fibers labeled predominantly at Cys^{707} with IATR of undocumented purity and isomer composition. These deflections were ~10-fold smaller than those obtained here in RLC-labeled fibers and may have been caused by motion artifacts.

The accompanying paper (Sabido-David et al., 1998a) reports the biochemical methodology and labeling protocols used here for labeling Cys^{108} of the RLC with the 5- and 6-isomers of IATR, exchange of the labeled RLC into muscle fibers, and steady-state fluorescence polarization measurements made in London on fibers in the relaxed, rigor, and contracting states. These observations were confirmed by data obtained on an independent fluorometer in Philadelphia and reported above. An earlier version of this instrument was used for measuring the time course of fluorescence polarization changes in muscle fibers during mechanical transients (Irving et al., 1995; Allen et al., 1996). In the present work, the apparatus was improved by the addition of *y* illumination, enabling measurement of the extent of nanosecond probe wobble.

The tilting of $Cys^{108\text{-}6}$ probes in response to a range of length step amplitudes was shown to be markedly nonlinear, strongly suggesting that a fraction of the myosin heads execute much larger angular changes than the estimated 3°–5° average tilt of the whole population (Irving et al., 1995, and discussed further below). The opposite sign of the length step response of $Cys^{108\text{-}6}$ probes in active contraction and rigor suggests a large change in probe angle, crossing the equatorial plane perpendicular to the fiber axis. The length step response of the $Cys^{108\text{-}5}$ probes, virtually absent in active contraction but appreciable in rigor, suggests that the RLC twists about its long axis between the active and rigor states. The experiments using caged ATP to switch fibers between rigor and active contraction reveal the time course of this transition.

Nanosecond probe wobble

Assuming that motions of the fluorescent probes with respect to the attached protein take place on a time scale faster than the ~5-ns fluorescence lifetime of rhodamine, we developed a method for estimating the extent of these motions. Irving (1996) presented equations describing the fluorescence polarization ratios expected for probes wobbling rapidly in a cone of half-angle δ. These equations were used in previous work (Ling et al., 1996; Allen et al., 1996; Sabido-David et al., 1998a) for analysis of the polarization ratios, but the extent of the fast probe motion was not measured. Here we added an independent set of measurements, using excitation light propagating perpendicular to the detector axis (*y* illumination, Fig. 1) that, in conjunction with in-line *x* illumination, allows estimation of δ (Eq. 2).

This analysis assumes that restricted motions of the probe relative to the protein domain to which it is attached are sufficiently rapid that the probe is equally likely to visit any angular position within a cone delimited by the half-angle δ during the ~5-ns fluorescence lifetime of ATR. Interdomain motions of the protein are likely to be considerably slower than this, and in the present measurements would contribute to the estimates of static disorder, σ in the Gaussian model, or *f* in the helix plus isotropic model. Motions on an intermediate time scale would contribute to both δ and either σ or *f*.

In the present work the extents of fast wobble were different for the two isomers of ATR bound to Cys^{108} (δ was ~20° for 6-ATR and ~25° for 5-ATR; Table 2), but did not depend on the contractile state of the fiber. These results are consistent with the interpretation of δ in terms of independent motions of the probe with respect to the light chain region of the myosin head, and suggest further that the local environment of the probes does not change between contractile states. Similar behavior of δ has been observed for the same two probe isomers bound to a series of five single-cysteine mutant skeletal RLCs exchanged into muscle fibers (Sabido-David et al., 1998b).

The orientation of the RLC region in relaxation, active contraction, and rigor

The steady-state values of fluorescence polarization ratios given here (Table 2) generally confirm those measured by Sabido-David et al. (1998a, their tables 2 and 3) on an independent fluorometer. A few quantitative discrepancies, mentioned in the Results, can be ascribed to the somewhat different experimental protocols. The main conclusions from the measurements of Sabido-David et al. (1998a) that are confirmed by the present results can be summarized as follows:

1. The 5- and 6-isomers of ATR have distinct orientations relative to the RLC region of the myosin head.
2. The orientation of the RLC region in rigor is clearly distinct from that in relaxation or active contraction.
3. The orientation of the RLC region in active contraction is similar but not identical to that in relaxation, and the difference cannot be explained by the presence of a population of probes in the rigor orientation.
4. Active contraction is characterized by an orientation different from that present in either relaxation or rigor.

These conclusions are discussed further by Sabido-David et al. (1998a).

Comparison of results from ATR probes on the RLC and at SH-1 on the myosin heavy chain

The orientations of 5- and 6-ATR bound to the most reactive cysteine residue in the catalytic domain of the myosin head (Cys^{707}, or SH-1) in active contraction were not intermediate between the corresponding orientations in relaxation and rigor (Berger et al., 1996), similar to the behavior of the ATR isomers on the RLC region. However, the orientation of spin labels bound to SH-1 in active contraction was consistent with a linear combination of the rigor and relaxed orientations (Cooke et al., 1982; Roopnarine and Thomas, 1995). This discrepancy between results from different probes bound to SH-1 suggests that some probes at that site change their orientation relative to the catalytic

domain as the contractile state is varied (Tanner et al., 1992; Berger et al., 1996).

The orientations of 5- and 6-ATR on SH-1 were very similar (Berger et al., 1996), in contrast to the distinct orientations of the two isomers on the RLC. The difference is presumably due to local interactions between the ATR isomers and the protein surfaces. Cys^{108} of chicken gizzard RLC is likely to be a surface residue (Rayment et al., 1993b; Xie et al., 1994), whereas Cys^{707} of the heavy chain is in a cleft (Rayment et al., 1993b), which may contribute to determining the probe orientation.

Torsional and axial changes of the RLC region between rigor and active contraction

In a rigor fiber the angle between the 5-ATR dipole and the fiber axis is ~20° less than the corresponding angle for the 6-ATR dipole (θ_g in Table 2; θ_g and θ_h in table 2 of Sabido-David et al., 1998a). In the transition from rigor to relaxation or to active contraction, the 6-ATR dipole becomes more parallel to the fiber axis, but the 5-ATR dipole becomes more perpendicular to it, so that the separation of the axial angles of the two isomers is only 5–8° (Sabido-David et al., 1998a). The difference between the angles of the two probes relative to the fiber axis would not change if the RLC underwent a purely axial rotation. The opposite behavior of the two ATR isomers suggests that the motion of the RLC region in this transition is not simply an axial rotation, but may involve a torsional motion of the RLC around its long axis (Sabido-David et al., 1998a). On other grounds, Cooke (1986) postulated a torsional motion of the region of the myosin head farthest from actin during the power stroke.

The responses of the two ATR isomers to length steps applied in rigor and active contraction support the idea of a torsional motion of the RLC between these two states, and suggest that the axial motion between the states might be considerably larger than that implied by steady-state fluorescence polarization measurements. Such measurements generally cannot distinguish between angles θ and $180° - \theta$ with respect to the symmetry axis of the sample. This ambiguity arises both from the dipolar nature of the absorption and emission optical transitions and from the twofold symmetry of the sarcomere about the equatorial plane perpendicular to the fiber axis. However, when changes in the polarization ratios are measured after length steps, the angles θ and $180° - \theta$ can be distinguished.

The change in orientation of the $Cys^{108\text{-}6}$ probes in response to a quick stretch in active contraction is in the direction opposite that in rigor (Irving et al., 1995; Figs. 2 and 6 here), suggesting that the probe dipoles that respond to the length step lie on opposite sides of the equatorial plane in the two states. If all of the probes in the fiber respond to the step, the change in orientation of the 6-ATR dipole between rigor and active contraction would be ~65°, taking $\theta_g = 61°$ in rigor and $(180 - 54)°$ in active contraction (Table 2). The mean angle change could be different from this if not all of the heads in the fiber respond to the length step, a possibility that is discussed more fully in a later section.

The changes in polarization ratios of $Cys^{108\text{-}5}$ probes in response to length steps in active contraction are very small (Fig. 3), suggesting that the 5-ATR dipole is nearly normal to the plane in which the long axis of the light chain region tilts (the tilt plane) in response to the length step. In contrast, the length step response of $Cys^{108\text{-}5}$ in rigor is very similar to that of $Cys^{108\text{-}6}$ (Fig. 6). The different response of the 5-ATR probe in active contraction and rigor might be caused by a change in the orientation of the probe relative to the RLC, but the observation that the extent of rapid probe wobble, δ, does not change appreciably makes this possibility unlikely. A more likely explanation is a torsional motion of the RLC between active contraction and rigor, as suggested earlier to explain the different steady-state orientations of the two isomers. Further experiments using bifunctional rhodamine probes with predefined orientation with respect to the RLC (Sabido-David et al., 1997; Hopkins et al., 1997) also suggest this torsional motion.

Elastic and active responses to length steps

The changes in polarization ratios in response to length steps had distinct time courses in active contraction and rigor. In rigor, Q ratios for both ATR isomers showed deflections during the length steps, but negligible changes after them (Fig. 6). The changes in Q ratios induced by quick stretches were reversible and had a roughly linear dependence on the size of the length step. Similar experiments with 5-ATR bound to SH-1 of the myosin heavy chain showed no change in the Q ratios during length steps, suggesting that the catalytic domain of the myosin head is rigidly attached to actin, although it is possible that the 5-ATR dipole is at an unfavorable angle for detecting axial motion (Berger et al., 1996). The motions reported by the RLC probes therefore indicate that elastic bending within the myosin head allows the RLC region to tilt. The flexible region may be at the interface between the catalytic and light chain regions.

In active contraction, deflections of the Q ratios were observed both during the length steps (corresponding to phase 1 of the tension transients) and during the quick phases of tension recovery (phase 2 of the tension transient). Thus the motions of the RLC region are related to both elastic properties and the conformational changes that are responsible for active force recovery after filament sliding. For small steps the deflections of $Q_\perp$ in phase 2 were in the same direction as those in phase 1 for both ATR isomers, although the phase 1 deflections were larger than those in phase 2 (Figs. 2–5). These results suggest that the RLC tilts further during active force recovery, and in the same direction as in the elastic response. For an active release the direction of tilting in both phases was toward the rigor

orientation. The 5- and 6-ATR probes at five other positions on chicken skeletal RLC also tilted toward their rigor orientations in active releases (Hopkins et al., 1996b; Sabido-David et al., 1998b).

In many of the present experiments, mechanical compliance at the ends of the fiber allowed sarcomere length changes to persist during phase 2 of the transients (Figs. 2 and 3). Tension recovered toward the isometric value during this period. Since the $Q_\perp$ ratios changed in the same direction during phase 2 as during the phase 1 in these examples, they might be detecting changes in the orientation of the RLC accompanying filament sliding rather than force generation per se. However, in experiments with negligible filament sliding during phase 2, the $Q_\perp$ ratios still showed deflections during phase 2 in the same direction as during phase 1, indicating that the phase 2 component is not caused by end compliance (see also Irving et al., 1995).

Nonlinearity of the length step response

In rigor, deflections of the *Q* ratios produced by length steps were generally proportional to the change in sarcomere length for both isomers, but in active contraction the relationship was markedly nonlinear. For $Cys^{108\text{-}6}$, the deflections of both ${}^{x}Q_\parallel$ and ${}^{x}Q_\perp$ saturated for releases of ~7 nm/h.s., and larger releases caused smaller deflections (Figs. 4 and 5). Applying the Gaussian orientation model with the assumption that all of the probes are distributed according to a single Gaussian peak, these results indicate an approximately linear decrease in peak angle, θ_g, of up to 6° for stretches of 7.5 nm/h.s. and a maximum increase of ~2° for releases of 7.5 nm/h.s. If tilting of the 10-nm myosin light chain region accounts for all of these applied length changes, the expected tilt angle is given approximately by $\tan^{-1}$ (7.5 nm/10 nm) = 37°, much greater than the values given by the Gaussian model. Several factors might reduce the observed tilt, such as an unfavorable angular disposition of the probe relative to the RLC, participation of less than 100% of the cross-bridges in the length step response, filament compliance, and incomplete recovery of tension after the length change.

The probes could be oriented at an angle that is unfavorable for detecting the motion; for instance, their dipoles may be oriented out of the tilt plane. However, in experiments similar to those presented here, using a series of five single-cysteine mutants of chicken skeletal RLC, labeled with either the 5- or 6-isomer of IATR, the angle changes produced by length changes were not larger than those obtained in the present work (Sabido-David et al., 1998b). It seems highly unlikely that all of these probes could be oriented at unfavorable angles.

Among all of the biochemical and mechanical states populated during a contraction, some would not be expected to tilt in response to the length steps (e.g., detached heads). Therefore the angular changes calculated assuming that the probe distribution is described by a single Gaussian model peak may greatly underestimate the tilting of the fraction that does move. The dependence of changes of ${}^{x}Q_\parallel$ and ${}^{x}Q_\perp$ on the amplitude of the length step (Figs. 4 and 5) is markedly nonlinear, which helps to quantitate the proportions of tilting and nontilting cross-bridges. A possible interpretation of this nonlinear behavior is that a release causes the 6-ATR dipoles to tilt away from the fiber axis and approach or cross the equatorial plane perpendicular to the fiber axis. Thus ${}^{x}Q_\perp$ increases for small releases, but reaches its maximum value for larger releases when the dipole reaches the 90° plane, and still larger releases produce a smaller change in ${}^{x}Q_\perp$. This interpretation is supported by the observation that for large releases, ${}^{x}Q_\perp$ recovers during phase 2 toward its isometric value (*inset* in Fig. 4, *trace 4*), in contrast to the continued change in the same direction as during phase 1 seen for smaller releases (*trace 1*). The angle changes of the probes that tilt in response to length changes are much greater than the average angle change. On this basis, amplitudes of the polarization ratio changes are relatively small, because a fraction of probes do not tilt in response to the length steps.

We estimated the fraction of tilting cross-bridges and nontilting cross-bridges by extending the Gaussian model of probe angular distribution to two components. A tilting fraction F is assumed to have a Gaussian distribution with peak angle θ_t, which changes when length steps are applied, and a constant width σ_t. In the isometric condition, the value of θ_t is θ_{t0}. If x is the translation of the myosin head-rod junction away from the position where $\theta_t = 90°$, then $\theta_t = \cos^{-1}(x/L_t)$, where L_t is the length of the tilting segment of the myosin head. The nontilting fraction $(1 - F)$ is assumed to have a peak angle θ_n and width σ_n. The six parameters required to describe this two-component model, F, θ_{t0}, σ_t, θ_n, σ_n, and L_t, lead to curves of expected change in ${}^{x}Q_\parallel$ and ${}^{x}Q_\perp$ versus size and direction of length step, which are fitted to corresponding experimental data (*smooth curves through the solid points* in Fig. 5 *A*). The fraction, F, and the isometric angle of the moving fraction of probes, θ_{t0}, are constrained by the slope and curvature of the plots in Fig. 5, whereas apparent length of the tilting region, L_t, is determined by the polarization ratios at the largest stretches and releases. Values obtained for the parameters fit to the data on the elastic response in Fig. 5 are $F = 12\%$, $\theta_{t0} = 60°$, $\sigma_t = 22°$, $\theta_n = 53°$, and $\sigma_n = 27°$. Estimating the sixth parameter, L_t, requires relating the motion at the head-rod junction, x, to changes in striation spacing. If we assume that half of the sarcomere compliance resides in the attached myosin heads and the other half in the myosin rod and the filaments, then $L_t = 9.4$ nm. If 25% of the sarcomere compliance were in the heads and 75% elsewhere, then L_t would be 4.7 nm.

The similar dependence of the model curves and data points on the amplitude of the length step indicates that the premise of a small fraction of probes tilting through a relatively large angle adequately explains the data. The fraction, F, of tilting probes estimated in this model is relatively insensitive to alignment of the probes with the

tilting plane, but θ_{t0} and L_t depend on the orientation of the probe dipoles relative to the tilting plane. The values given above depend on the particular assumptions of the model, and thus should be taken only as guidelines that serve to illustrate that the data can be explained by a small fraction of probes tilting by a relatively large angle. Assuming that half of the sarcomere compliance is in the heads, a step release of 9.4 nm that translates the head-rod junction by 4.7 nm tilts the moving 12% of the probes from 60° to 90°. Larger releases tilt the probes beyond 90°. The same wide range of length steps as shown in Fig. 5 was examined in one other experiment. Very similar values of the fitted model parameters were obtained.

The nontilting fraction of probes (~88% for Fig. 5) may be on detached cross-bridges, but some attached cross-bridges may also be included. If they quickly detach as they reach the end of their working stroke during the transient, attached cross-bridges would not contribute fully to the response. Weakly attached cross-bridges that have not entered the working stroke may also detach quickly when the length change is applied.

The polarization ratios after the quick recovery can be qualitatively explained on the same basis. After the step, the probes continue tilting in the same direction as during the step. This tilting during quick tension recovery results in further deflections of the *Q* signals, except for the largest releases, where further tilting beyond 90° reduces the deflections, as observed. However, the simple geometric model described for the elastic response did not fit the quick recovery data as well, indicating that further processes (e.g., nonlinear extent of active tilting, cross-bridge detachment, etc.) take place.

Nonlinearity of the $Cys^{108\text{-}5}$ length step response in active contraction is apparent as tilting in the same direction for stretches as for releases (Fig. 3). This could be explained by probes tilting away from the equatorial plane, although it is unlikely that a large proportion of the probes could be at 90° during active contraction, because the peak angle for $Cys^{108\text{-}5}$ is <50° (Table 2). The possibility that a moving fraction of 5-ATR dipoles is oriented along the fiber axis is made unlikely by the negative deflections of ${}^{x}Q_{\perp}$ and ${}^{y}Q_{\perp}$, indicating probe motions toward the fiber axis.

The length step response of $Cys^{108\text{-}6}$ probes in rigor was linear in the range of length steps tested (approximately −0.5 to +3 nm/h.s.; data not shown). A two-component model similar to that described above for active contraction data could be fitted to the rigor length step data, but the model parameters were not constrained to unique values. For instance, 90% of the cross-bridges tilting 0.4°/nm/h.s. of length change or 20% tilting 1.8°/nm/h.s. are consistent with the polarization ratio changes. In this model, values of the tilting fraction lower than 20% were not consistent with the data, because the calculated dependence of *Q* changes on length step amplitude became markedly nonlinear. Thus more rigor cross-bridges seem to respond to imposed length steps than active cross-bridges, as expected from the higher stiffness in rigor.

Properties of attached cross-bridges before force generation

The opposite stretch response of $Cys^{108\text{-}6}$ in rigor and active isometric contraction allows us to investigate the dynamics of the transition between these two states in the cross-bridge cycle. When the fiber is switched from rigor to active contraction by photolysis of caged ATP in the presence of Ca^{2+}, the *Q* ratios change first (see also Allen et al., 1996), then the stretch response becomes like that in active contraction, and finally, force development ensues. This sequence provides evidence for an initial state of cross-bridge attachment, before force generation, that nevertheless responds to length changes in the same way as the steady-state active cross-bridges. When the amount of photoliberated ATP is reduced, all three of these signals are slowed, and the changes in kinetics are accounted for simply by the slower rate of ATP binding (Fig. 9). In a sequence of linked reactions with similar rate constants, as in the cross-bridge cycle, several processes may determine the overall reaction rate, detected here as the rate of force development. In our experimental conditions, with [ATP] ≤ 1 mM, the final development of force is apparently controlled by several processes: the rate of ATP binding, attachment of cross-bridges (probably weakly bound) that do not contribute force, and the transition into the force-generating state. Filament sliding due to series compliance within the sarcomeres or at the fiber ends may also affect the rate of force development.

In muscle relaxed at low ionic strength, the high-frequency stiffness of the fiber is high (Brenner et al., 1982), and the equatorial x-ray diffraction pattern indicates considerable cross-bridge mass near the actin filaments (Brenner et al., 1984). These observations have been interpreted as indicating the attachment of cross-bridges in a state similar to the preforce attachments discussed above (Brenner, 1987). Although the changes in *Q* ratios are small, the stretch response of the attached cross-bridges under these low ionic strength conditions (Fig. 7) is in the same direction as the active stretch response (Fig. 2). This result is consistent with the results of the caged ATP experiment indicating preforce attachments with the active-type stretch response (Fig. 9). Together, these results support the hypothesis that cross-bridges attached to actin filaments in fibers relaxed at low ionic strength are structurally similar to the initial, preforce cross-bridges present during normal contraction.

However, the steady-state values of fluorescence polarization ratios in the low ionic strength relaxing solution are consistent with a mixture of populations of probe dipole orientations characteristic of normal ionic strength relaxing and rigor solutions (Sabido-David et al., 1998a, and Table 2 of this paper), with no evidence of a component with the orientation distribution characteristic of active contraction. The steady-state and length step results may be rationalized if there are at least two populations of cross-bridges in low ionic strength relaxing solution, one at the rigor orientation

with the rigor stretch response and another, larger group at the active orientation with the active stretch response. The combination of these two populations with opposite signs of stretch response would lead to small changes in the *Q* ratios after a stretch, as observed (Fig. 7).

SUMMARY

Fluorescence polarization measurements cannot generally distinguish probe angles θ and $180° - \theta$, because the probes and biological preparations have twofold symmetry. The angular discrimination afforded by imposing a nonsymmetrical strain with the length steps is unique to this preparation and allows us to distinguish between cross-bridge populations on either side of the equatorial plane, according to their response to the applied length changes. With relatively simple optical arrangements, not requiring nanosecond time resolution, the extent of probe motions on the nanosecond time scale of the fluorescence lifetime can be measured. The results suggest that the cross-bridge cycle involves an initial attachment to actin with structural similarities to the force-generating cross-bridge, and that force generation occurs in a subsequent transition in the attached head (Huxley and Simmons, 1971). Cross-bridges attached in muscle relaxed at low ionic strength share some structural features with these preforce attachments. Fluorescence polarization changes in response to length steps in active contractions were relatively small in amplitude but markedly nonlinear, suggesting that a small fraction of cross-bridges (~10%) undergo angle changes of 30° or more when step releases are applied. The two isomers of acetamidotetramethylrhodamine are useful in distinguishing cross-bridge states and motions in the plane of the muscle fiber axis (axial motions or tilting) and around the long axis of the RLC (twisting). The transitions between the relaxed, contracting, and rigor states seem to involve twisting as well as tilting of the light chain region of the myosin head.

The authors thank Mr. Joseph Pili for excellent mechanical construction, and Mr. Le Phan, Mr. Piyush Tantia, and Mr. Joel Saunders for software support.

The work was supported by NIH Grant AR26846 to YEG; the MDA, MRC, Wellcome Trust, UK; and an American Heart Association Pre-Doctoral Fellowship to SCH.

REFERENCES

Allen, T. St. C., N. Ling, M. Irving, and Y. E. Goldman. 1996. Orientation changes in myosin regulatory light chains following photorelease of ATP in skinned muscle fibers. *Biophys. J.* 70:1847–1862.

Barabás, K., and L. Keszthelyi. 1984. Temperature dependence of ATP release from "caged" ATP. *Acta Biochim. Biophys. Acad. Sci. Hung.* 19:305–309.

Berger, C. L., J. S. Craik, D. R. Trentham, J. E. T. Corrie, and Y. E. Goldman. 1996. Fluorescence polarization of skeletal muscle fibers labeled with rhodamine isomers on the myosin heavy chain. *Biophys. J.* 71:3330–3343.

Borejdo, J., and S. Putnam. 1977. Polarization of fluorescence from single skinned glycerinated rabbit psoas fibers in rigor and relaxation. *Biochim. Biophys. Acta.* 459:578–595.

Brenner, B. 1987. Mechanical and structural approaches to correlation of cross-bridge action in muscle with actomyosin ATPase in solution. *Annu. Rev. Physiol.* 49:655–672.

Brenner, B., M. Schoenberg, J. M. Chalovich, L. E. Greene, and E. Eisenberg. 1982. Evidence for cross-bridge attachment in relaxed muscle at low ionic strength. *Proc. Natl. Acad. Sci. USA.* 79:7288–7291.

Brenner, B., L. C. Yu, and R. J. Podolsky. 1984. X-ray diffraction evidence for cross-bridge formation in relaxed muscle fibers at various ionic strengths. *Biophys. J.* 46:299–306.

Burghardt, T. P., S. P. Garamszegi, and K. Ajtai. 1997. Probes bound to myosin Cys-707 rotate during length transients in contraction. *Proc. Natl. Acad. Sci. USA.* 94:9631–9636.

Cecchi, G., F. Colomo, and V. Lombardi. 1976. A loudspeaker servo system for determination of mechanical characteristics of isolated muscle fibres. *Boll. Soc. It. Biol. Sper.* 52:733–736.

Chase, P. B., and M. J. Kushmerick. 1988. Effects of pH on contraction of rabbit fast and slow skeletal muscle fibers. *Biophys. J.* 53:935–946.

Chen, R. F., and R. L. Bowman. 1965. Fluorescence polarization: measurement with ultraviolet-polarizing filters in a spectrophotofluorometer. *Science.* 147:729–732.

Ciarcia, S. 1981a. Build a Z8-based control computer with BASIC, Part 1. *BYTE Mag.* 6:146–155.

Ciarcia, S. 1981b. Build a Z8-based control computer with BASIC, Part 2. *BYTE Mag.* 6:156–166.

Cooke, R. 1986. The mechanism of muscle contraction. *CRC Crit. Rev. Biochem.* 21:53–118.

Cooke, R., M. S. Crowder, and D. D. Thomas. 1982. Orientation of spin labels attached to cross-bridges in contracting muscle fibres. *Nature.* 300:776–778.

Cooke, R., M. S. Crowder, C. H. Wendt, V. A. Barnett, and D. D. Thomas. 1984. Muscle cross-bridges: do they rotate? *In* Contractile Mechanisms in Muscle. G. H. Pollack and H. Sugi, editors. Plenum Press, New York. 413–427.

Corrie, J. E. T., and J. S. Craik. 1994. Synthesis and characterisation of pure isomers of iodoacetamidotetramethylrhodamine. *J. Chem. Soc., Perkin Trans. 1.* 2967–2973.

Dale, R. E., T. Marszalek, S. C. Hopkins, M. Irving, and Y. E. Goldman. 1997. Model-independent analysis of mobility and orientation of fluorescent probes in muscle fibers. *Biophys. J.* 72:A52 (Abstr.).

Finer, J. T., R. M. Simmons, and J. A. Spudich. 1994. Single myosin molecule mechanics: piconewton forces and nanometre steps. *Nature.* 368:113–119.

Goldman, Y. E. 1987. Measurement of sarcomere shortening in skinned fibers from frog muscle by white light diffraction. *Biophys. J.* 52:57–68.

Goldman, Y. E., M. G. Hibberd, and D. R. Trentham. 1984a. Relaxation of rabbit psoas muscle fibres from rigor by photochemical generation of adenosine-5′-triphosphate. *J. Physiol. (Lond.)* 354:577–604.

Goldman, Y. E., M. G. Hibberd, and D. R. Trentham. 1984b. Initiation of active contraction by photogeneration of adenosine-5′-triphosphate in rabbit psoas muscle fibres. *J. Physiol. (Lond.)* 354:605–624.

Goldman, Y. E., and R. M. Simmons. 1984. Control of sarcomere length in skinned muscle fibres of *Rana temporaria* during mechanical transients. *J. Physiol. (Lond.)* 350:497–518.

Gollub, J., C. R. Cremo, and R. Cooke. 1996. ADP release produces a rotation of the neck region of smooth myosin but not skeletal myosin. *Nature Struct. Biol.* 3:796–802.

Hopkins, S. C., L. Phan, M. Irving, and Y. E. Goldman. 1995. Oscillations in the orientation of acetamidotetramethylrhodamine (ATR) probes on myosin regulatory light chain (RLC) caused by sinusoidal length changes in skinned muscle fibers. *Biophys. J.* 68:A9 (Abstr.).

Hopkins, S. C., C. Sabido-David, B. D. Brandmeier, J. Kendrick-Jones, R. E. Dale, J. E. T. Corrie, D. R. Trentham, M. Irving, and Y. E. Goldman. 1997. Motions of bifunctional rhodamine probes with defined orientations on the regulatory light chain (RLC) in skeletal muscle fibers. *Biophys. J.* 72:A1 (Abstr.).

Hopkins, S. C., C. Sabido-David, M. Irving, and Y. E. Goldman. 1996a. Repriming of tilting in the myosin light-chain region following length steps in muscle fibers. *Biophys. J.* 70:A291 (Abstr.).

Hopkins, S. C., C. Sabido-David, L. D. Saraswat, Y. E. Goldman, M. Irving, and S. Lowey. 1996b. Tilting motions of rhodamine probes at five different sites on the myosin regulatory light chain (RLC) following length steps in contracting muscle fibers. *Biophys. J.* 70:A17 (Abstr.).

Huxley, A. F., and R. M. Simmons. 1971. Proposed mechanism of force generation in striated muscle. *Nature.* 233:533–538.

Irving, M. 1996. Steady-state polarization from cylindrically symmetric fluorophores undergoing rapid restricted motion. *Biophys. J.* 70: 1830–1835.

Irving, M., T. St. C. Allen, C. Sabido-David, J. S. Craik, B. Brandmeier, J. Kendrick-Jones, J. E. T. Corrie, D. R. Trentham, and Y. E. Goldman. 1995. Tilting of the light-chain region of myosin during step length changes and active force generation in skeletal muscle. *Nature.* 375: 688–691.

Irving, M., V. Lombardi, G. Piazzesi, and M. A. Ferenczi. 1992. Myosin head movements are synchronous with the elementary force-generating process in muscle. *Nature.* 357:156–158.

Ling, N., C. Shrimpton, J. Sleep, J. Kendrick-Jones, and M. Irving. 1996. Fluorescent probes of the orientation of myosin regulatory light chains in relaxed, rigor, and contracting muscle. *Biophys. J.* 70:1836–1846.

Lombardi, V., and G. Piazzesi. 1990. The contractile response during steady lengthening of stimulated frog muscle fibres. *J. Physiol. (Lond.)* 431:141–171.

Lombardi, V., G. Piazzesi, M. A. Ferenczi, H. Thirlwell, I. Dobbie, and M. Irving. 1995. Elastic distortion of myosin heads and repriming of the working stroke in muscle. *Nature.* 374:553–555.

Lowey, S., G. S. Waller, and K. M. Trybus. 1993. Skeletal muscle myosin light chains are essential for physiological speeds of shortening. *Nature.* 365:454–456.

Martyn, D. A., and P. B. Chase. 1995. Faster force transient kinetics at submaximal Ca^{2+} activation of skinned psoas fibers from rabbit. *Biophys. J.* 68:235–242.

Molloy, J. E., J. E. Burns, J. Kendrick-Jones, R. T. Tregear, and D. C. S. White. 1995. Movement and force produced by a single myosin head. *Nature.* 378:209–212.

Morales, M. F., J. Borejdo, J. Botts, R. Cooke, and R. A. Mendelson. 1982. Some physical studies of the contractile mechanism in muscle. *Annu. Rev. Phys. Chem.* 33:319–351.

Ostap, E. M., V. A. Barnett, and D. D. Thomas. 1995. Resolution of three structural states of spin-labeled myosin in contracting muscle. *Biophys. J.* 69:177–188.

Press, W. H., S. A. Teukolsky, W. T. Vetterling, and B. P. Flannery. 1992. Numerical Recipes in C. The Art of Scientific Computing. Cambridge University Press, New York. 683–688.

Rayment, I., H. M. Holden, M. Whittaker, C. B. Yohn, M. Lorenz, K. C. Holmes, and R. A. Milligan. 1993a. Structure of the actin-myosin complex and its implications for muscle contraction. *Science.* 261: 58–65.

Rayment, I., W. R. Rypniewski, K. Schmidt-Bäse, R. Smith, D. R. Tomchick, M. M. Benning, D. A. Winkelmann, G. Wesenberg, and H. M. Holden. 1993b. Three-dimensional structure of myosin subfragment-1: a molecular motor. *Science.* 261:50–58.

Roopnarine, O., and D. D. Thomas. 1995. Orientational dynamics of indane dione spin-labeled myosin heads in relaxed and contracting skeletal muscle fibers. *Biophys. J.* 68:1461–1471.

Sabido-David, C., B. D. Brandmeier, J. S. Craik, J. E. T. Corrie, D. R. Trentham, and M. Irving. 1998a. Steady-state fluorescence polarization studies of the orientation of myosin regulatory light chains in single skeletal muscle fibers using pure isomers of iodoacetamidotetramethylrhodamine. *Biophys. J.* 74:3083–3092.

Sabido-David, C., R. E. Ferguson, B. D. Brandmeier, S. C. Hopkins, Y. E. Goldman, J. Kendrick-Jones, R. E. Dale, J. E. T. Corrie, D. R. Trentham, and M. Irving. 1997. Orientation of bifunctional rhodamine probes on myosin regulatory light chain (RLC) in relaxed, contracting and rigor muscle. *Biophys. J.* 72:A52 (Abstr.).

Sabido-David, C., S. C. Hopkins, L. D. Saraswat, S. Lowey, Y. E. Goldman, and M. Irving. 1998b. Orientation changes of fluorescent probes at five sites on the myosin regulatory light chain during contraction of single skeletal muscle fibres. *J. Mol. Biol.* 275:387–402.

Savitzky, A., and M. J. E. Golay. 1964. Smoothing and differentiation of data by simplified least squares procedures. *Anal. Chem.* 36:1627–1639.

Schwartz, M. 1959. Information Transmission, Modulation, and Noise. A Unified Approach to Communication Systems. McGraw-Hill, New York. p. 160.

Tanner, J. W., D. D. Thomas, and Y. E. Goldman. 1992. Transients in orientation of a fluorescent cross-bridge probe following photolysis of caged nucleotides in skeletal muscle fibres. *J. Mol. Biol.* 223:185–203.

Tregear, R. T., and R. A. Mendelson. 1975. Polarization from a helix of fluorophores and its relation to that obtained from muscle. *Biophys. J.* 15:455–467.

Uyeda, T. Q. P., P. D. Abramson, and J. A. Spudich. 1996. The neck region of the myosin motor domain acts as a lever arm to generate movement. *Proc. Natl. Acad. Sci. USA.* 93:4459–4464.

VanBuren, P., G. S. Waller, D. E. Harris, K. M. Trybus, D. M. Warshaw, and S. Lowey. 1994. The essential light chain is required for full force production by skeletal muscle myosin. *Proc. Natl. Acad. Sci. USA.* 91:12403–12407.

van Gurp, M., T. van Heijnsbergen, G. van Ginkel, and Y. K. Levine. 1989. Determination of transition moment directions in molecules of low symmetry using polarized fluorescence. II. Applications to pyranine, perylene, and DPH. *J. Chem. Phys.* 90:4103–4111.

Walker, J. W., G. P. Reid, and D. R. Trentham. 1989. Synthesis and properties of caged nucleotides. *Methods Enzymol.* 172:288–301.

Whittaker, M., E. M. Wilson-Kubalek, J. E. Smith, L. Faust, R. A. Milligan, and H. L. Sweeney. 1995. A 35-Å movement of smooth muscle myosin on ADP release. *Nature.* 378:748–753.

Xie, X., D. H. Harrison, I. Schlichting, R. M. Sweet, V. N. Kalabokis, A. G. Szent-Györgyi, and C. Cohen. 1994. Structure of the regulatory domain of scallop myosin at 2.8 Å resolution. *Nature.* 368:306–312.